Check for updates

Received: 16 December 2021 | Revised: 5 April 2022 | Accepted: 7 April 2022

DOI: 10.1002/esp.5383

RESEARCH ARTICLE

ESPL WILEY

Topographic controls on ice flow and recession for Juneau Icefield (Alaska/British Columbia)

Bethan Davies[1] | Jacob Bendle[2] | Jonathan Carrivick[3] | Robert McNabb[4] | Christopher McNeil[5] | Mauri Pelto[6] | Seth Campbell[7] | Tom Holt[8] | Jeremy Ely[9] | Bradley Markle[10]

[1]Centre for Quaternary Research, Department of Geography, Royal Holloway University of London, Egham, UK

[2]Geography Program, University of Northern British Columbia, Prince George, Canada

[3]School of Geography and water@leeds, University of Leeds, Leeds, UK

[4]School of Geography and Environmental Sciences, Ulster University, Newtonabbey, UK

[5]US Geological Survey, Alaska Science Centre, Anchorage, AK, USA

[6]Nichols College, Dudley, Massachusetts, USA

[7]School of Earth and Climate Sciences/Climate Change Institute, University of Maine, Orono, Maine, USA

[8]Centre for Glaciology, Department of Geography and Earth Sciences, Aberystwyth University, Aberystwyth, UK

[9]Department of Geography, University of Sheffield, Sheffield, UK

[10]Geological Sciences, University of Colorado Boulder, Boulder, Colorado, USA

Correspondence
Bethan Davies, Centre for Quaternary Research, Department of Geography, Royal Holloway University of London, Egham TW20 0EX, UK.
Email: bethan.davies@rhul.ac.uk

Funding information
Royal Holloway University of London

Abstract

Globally, mountain glaciers and ice caps are losing dramatic volumes of ice. The resultant sea-level rise is dominated by contributions from Alaska. Plateau icefields may be especially sensitive to climate change due to the non-linear controls their topography imparts on their response to climate change. However, Alaskan plateau icefields have been subject to little structural glaciological or regional geomorphological assessment, which makes the controls on their present and former mass balance difficult to ascertain.

We inventoried 1050 glaciers and 368 lakes in the Juneau Icefield region for the year 2019. We found that 63 glaciers had disappeared since the 2005 inventory, with a reduction in glacier area of 422 km^2 (10.0%). We also present the first structural glaciological and geomorphological map for an entire icefield in Alaska. Glaciological mapping of >20 800 features included crevasses, debris cover, foliation, ogives, medial moraines and, importantly, areas of glacier fragmentation, where glaciers either separated from tributaries via lateral recession ($n = 59$), or disconnected within areas of former icefalls ($n = 281$). Geomorphological mapping of >10 200 landforms included glacial moraines, glacial lakes, trimlines, flutes and cirques. These landforms were generated by a temperate icefield during the Little Ice Age (LIA) neoglaciation. These data demonstrate that the present-day outlet glaciers, which have a similar thermal and ice-flow regime, have undergone largely continuous recession since the LIA. Importantly, disconnections occurring within glaciers can separate accumulation and ablation zones, increasing rates of glacier mass loss. We show that glacier disconnections are widespread across the icefield and should be critically taken into consideration when icefield vulnerability to climate change is considered.

KEYWORDS
crevasse, geomorphology, glacier, mass balance, moraine, structural glaciology

1 | INTRODUCTION

1.1 | Rationale and aims

Glaciers distinct from the Antarctic and Greenland ice sheets lost 271 ± 23 billion tonnes of ice per year from 2005 to 2014 (Hugonnet et al., 2021), driving 21% of global observed sea-level rise (Hugonnet et al., 2021; Jakob et al., 2021; Slater et al., 2021; Zemp et al., 2019). This loss of glacier ice volume was 1.5 times the ice lost in the same period from the Greenland Ice Sheet, and twice that lost from the Antarctic Ice Sheet (Hugonnet et al., 2021). Losses from Alaska account for a full quarter of all the ice lost from global glaciers (Hugonnet

This is an open access article under the terms of the Creative Commons Attribution License, which permits use, distribution and reproduction in any medium, provided the original work is properly cited.
© 2022 The Authors. *Earth Surface Processes and Landforms* published by John Wiley & Sons Ltd. This article has been contributed to by U.S. Government employees and their work is in the public domain in the USA.

et al., 2021; Zemp et al., 2019), making this the largest contributor of the Randolph Glacier Inventory (RGI) regions (as defined by Peffer et al. (2014) and the Randolph Glacier Inventory et al., 2017). This trend is projected to continue throughout the 21st century (Edwards et al., 2021; Marzeion et al., 2020; Shannon et al., 2019).

Alaska contains several large plateau icefields, such as Juneau Icefield, Harding Icefield and Stikine Icecap. Plateau icefields are characterized by their large, interconnected, low-slope accumulation areas and top-heavy hypsometry (Furbish & Andrews, 1984; McGrath et al., 2017). They are susceptible to rapid recession and downwasting of their outlet glaciers once equilibrium line altitudes (ELAs) reach the edge of the plateau, because small ELA changes lead to a large change in the accumulation area (Barr & Lovell, 2014; Boston & Lukas, 2019; McGrath et al., 2017; Oerlemans, 1989). These top-heavy ice masses are predicted to experience significant area loss over coming decades (Åkesson et al., 2017; McGrath et al., 2017; Zekollari et al., 2017; Ziemen et al., 2016).

Structural glaciological mapping provides insights into flow regime, glacier dynamics and mass balance (Hambrey & Clarke, 2019; Hambrey & Lawson, 2000; Jennings & Hambrey, 2021; Jennings et al., 2014, 2016). Crevasses influence surface mass balance by increasing surface roughness, as well as latent and sensible heat fluxes, resulting in increased ablation. Crevassing and moulins on the ice surface can also provide a pathway of glacier surface water to the bed, decreasing effective pressure and enhancing basal sliding (Colgan et al., 2016).

However, to date, structural mapping has generally focused on valley glaciers (e.g. Azzoni et al., 2017; Goodsell et al., 2002; Goodsell, Hambrey, & Glasser, 2005; Goodsell, Hambrey, Glasser, Nienow, et al., 2005; Jennings & Hambrey, 2021; Kellerer-Pirklbauer & Kulmer, 2019; Lovell et al., 2015) or surging glaciers (Hambrey & Clarke, 2019), rather than regional or icefield scales. Further, thinning of ice across bedrock steps in icefalls or heavily crevassed areas can result in 'detachments' or 'disconnections' between accumulation and ablation areas of a glacier, driving glacier tongue stagnation and exacerbated recession (Boston & Lukas, 2019; Jiskoot et al., 2009; Rippin et al., 2020). An icefield-wide assessment of these important new structures is critically required in order to assess their prevalence, importance and controls on their occurrence. Finally, since glacier structures can influence glacier mass balance (Colgan et al., 2016) and control icefield fragmentation, their mapping can shed insights into the controls on glacier recession.

In terms of glacial geomorphology, a landsystems approach can provide insights into how glaciers have behaved under former climatic regimes, and can yield information on the controls on glacier behaviour. However, to date, analysis of plateau icefield geomorphology has focused on glaciers in Iceland, Scotland or Norway (Bickerdike et al., 2018; Boston & Lukas, 2019; Boston et al., 2015; Bradwell et al., 2013; Chandler et al., 2019; Evans, 2010; Evans et al., 2002, 2006, 2016; Weber et al., 2019), which all have different thermal regimes and mass-balance characteristics to Alaskan icefields. Icelandic outlet glaciers are typically less confined to valleys than Alaskan icefield outlet glaciers. This means that in Iceland, the development of true valley glaciers with higher velocities than the plateau area is limited. Icelandic ice caps therefore tend to be thinner and outlet glaciers have lower velocities than those in Alaska (excepting a small number of southern outlet glaciers of Vatnajökull). Norway's plateau glaciers have a lower velocity and thinner glaciers emanating from smaller plateaus. These differences are evident in recent velocity and ice thickness datasets (Millan et al., 2022). A detailed glacial landsystems analysis of North American plateau icefields is markedly absent from the literature.

This study aims to inventory glacier extent and structural characteristics of the Juneau Icefield region in 2019 AD and to capture Little Ice Age (LIA) glacial geomorphology. We combine for the first time in NW North America analyses of glacial geomorphology, glacial lakes and structural glaciology to gain insights into the dynamics of flow regime and controls on glacier change, both today and during the LIA. These data highlight the topographic controls driving icefield disconnections and fragmentations, which are not well represented in numerical models. The full dataset is available as ESRI Shapefiles and an A0 map within the online Supplementary Information.

1.2 | Juneau Icefield study area

Juneau Icefield (Figure 1) is a plateau icefield on the northern Coast Mountains (58.6°N, 134.5°W), straddling the boundary between Alaska and British Columbia. Juneau Icefield is among the largest icefields in the world. Glacier elevations range from 0 to 2300 m a.s.l. The icefield has a large, low-slope accumulation area at ~1200–2300 m (~1400 km^2), drained by topographically confined outlet glaciers (Sprenke et al., 1999b) (Figure 1). The interconnected low-slope area of the icefield lies above 1500 m on Tulsequah Glacier in the east, and above 1200 m over Taku, Norris, West and East Twin and Field Glacier in the south. Although extensive research on the glacier area, mass balance, volume change and glaciology of the icefield and its environs has been undertaken since the 1940s (e.g. Berthier et al., 2018; Heusser, 1954; Kaufman et al., 2011; Larsen et al., 2007; McNeil et al., 2020; Nagorski et al., 2019; O'Neel et al., 2019; Pelto, 2019; Pelto et al., 2013; Sprenke et al., 1999a; Veitch et al., 2021; Ziemen et al., 2016), the structural glaciology has not yet been analysed.

Observational data of temperatures from Juneau Airport meteorological station (Figure 1) show 1986–2005 mean annual air temperatures of 5.8°C, reaching 13.4°C mean summer air temperatures (NOAA, 2021; station USW00025309). The icefield occupies a zone of intense climate transition, ranging from temperate maritime in the west to continental in the much drier east (NOAA, 2021; Roth et al., 2018). There was an increase in mean annual air temperatures of 1.13°C in the decades from 2001 to 2020 relative to 1941–1970, and an increase in mean summer temperatures of 0.97°C over the same time periods. For mean annual air temperatures, 6 of the 10 warmest years have occurred since the year 2000, and the 10 coolest years all occurred prior to 1973. The year 2019, the year of our survey, was one of these 10 warmest years, with a temperature anomaly of +1.58°C relative to the 1986–2005 mean. This trend is in line with observations across Alaska (Thoman & Walsh, 2019), which shows warming temperatures since the 1970s, exceptionally warm recent years and a longer melt season.

Measured ELAs (2011–2020) now average 1297 m (SD 324 m) on Lemon Creek and 1172 m (SD 150 m) for Taku Glacier (McNeil et al., 2016, 2020). Higher ELAs over Lemon Creek Glacier have been reported, rising above the glacier's Z_{max} of 1500 m in 2018 and 2019 (data from McNeil et al., 2016). The mean ELA has risen by 200 m since the 1953–1960 mean. The ELA of Taku Glacier reached 1308 m in 2018, and a record high of 1528 m in 2019 (McNeil et al., 2016, 2020).

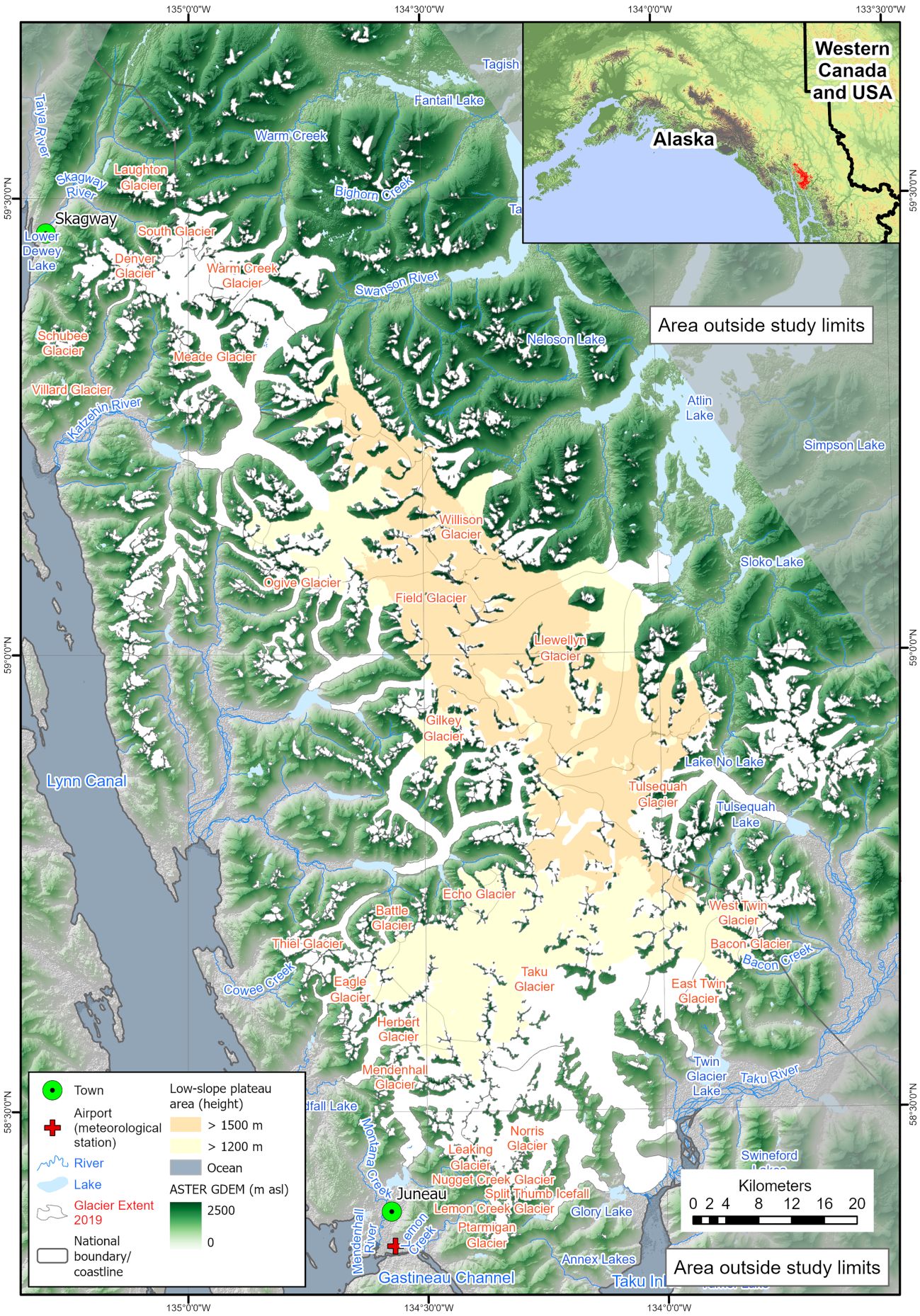


FIGURE 1 Legend on next page.

FIGURE 1 Juneau Icefield in 2019, with key glacier names and placenames used in the text. The interconnected plateau area, with slope <10° and ice above 1500 and 1200 m, is shaded pale yellow and orange. Overlain on hillshaded ASTER GDEM. Inset (top right) shows the RGI region of Alaska (thick black line) with Juneau Icefield highlighted in red. Alaskan glaciers (grey) are from the Randolph Glacier Inventory (RGI) (Pfeffer et al., 2014; Randolph Glacier Inventory Consortium et al., 2017). [Color figure can be viewed at wileyonlinelibrary.com]

TABLE 1 Details of previous work dating LIA moraines around Juneau Icefield

Glacier	Year of neoglacial moraine formation	Details	References
Taku	AD 1750–1755	Near Taku Point, blocking Taku Inlet and Taku River, forming an ice-dammed lake Radiocarbon dating of peat overlying lacustrine clays near Loon Lakes, west of Taku Glacier; dendrochronology and radiocarbon at Taku Point	Lawrence (1950); Miller (1964); Motyka and Begét (1996)
Llewellyn	Minimum age for moraines; 1210–430 cal. years BP (AD 740–1520)	Dated by radiocarbon of overridden twigs and tree stumps in small lakes	Clague et al. (2010)
Tulsequah	Minimum age for moraine; 1458 AD	Dated by radiocarbon dating of tree stem of glacially overridden tree	Clague et al. (2010)
Herbert	AD 1765		Lawrence (1950)
Eagle	AD 1785–1790	Dated by dendrochronology	Knopf (1912)
Lemon Creek	AD 1750	Dated by dendrochronology	Heusser and Marcus (1964)

1.3 | Late Holocene neoglaciation of Juneau Icefield

Across Alaska, there is widespread evidence of a Late Holocene neoglaciation—the LIA (Koch & Clague, 2011; Molnia, 2007; Motyka, 2003; Porter, 2013; Wiles et al., 1999). Advances dating from the middle 1700s to late 1800s dominate, and were frequently the most extensive of the last 10 000 years (Calkin, 1988; Koch & Clague, 2011). Many glaciers in Alaska below 1500 m a.s.l. have an uninterrupted history of continuous recession since this maximum (Molnia, 2007). There is substantial evidence of a readvance of glaciers around Juneau Icefield during the LIA, ending between ca. 1750 to 1786 (Table 1) (Knopf, 1912; Lawrence, 1950; Miller, 1964; Motyka & Begét, 1996; Röthlisberger, 1986; Wentworth & Ray, 1936).

Local relative sea-level data indicate that larger-than-present glaciers had stabilized by the mid-16th century, with land first emerging due to isostatic rebound as glaciers shrank between AD 1770–1790 (Motyka, 2003). Glaciers have been consistently shrinking since this maximum (Miller, 1964). The exception is Taku Glacier, a tidewater glacier and the largest outlet glacier of Juneau Icefield, which, after advancing since the late 19th century, has been shrinking since 2013 (McNeil et al., 2020). Taku Glacier calved along its entire terminus until 1948, after which time a shoal terminal moraine was formed above sea level (Kuriger et al., 2006). After this, ice-proximal moraines developed along the lobate terminus, preventing contact with warm ocean water, calving and submarine melting (Kuriger et al., 2006).

2 | MATERIALS AND METHODS

2.1 | Data sources

Glaciers, ice-surface structures and glacial lakes of the Juneau Icefield region were manually mapped in ESRI ArcGIS Pro (projection WGS 84, UTM zone 8 N), using 10 m-resolution Sentinel-2 imagery (swath 290 km), with a map produced at 1:10 000 scale. Six overlapping images were selected from 30 August to 7 September 2019, which provided clear coverage of the entire icefield, with limited cloud or snow cover due to the exceptional record-high late-summer snowline that year (Table 2) (McNeil et al., 2016, 2019). Composite true colour and black and white band 4 imagery were both used to visualize glacier outlines, structures and landforms. The short timeframe between image acquisitions allowed temporal continuity of mapping over the entire icefield. Higher-resolution ESRI Basemap imagery from June 2020 was additionally used to cross-check some features.

Topographic data were derived from the 2 m-resolution ArcticDEM v3.0 release 7 (Porter et al., 2018) using the 30 m ASTER GDEM v3.0 to fill voids (ASTER GDEM Validation Team et al., 2009). Hillshade, aspect and slope models were derived from the composite digital elevation model (DEM) mosaic to aid interpretation of glaciological features and to calculate elevation, slope and aspect parameters for each glacier.

2.2 | Glacier outlines

Glacier outlines were initially derived from the Randolph Glacier Inventory (RGI) version 6.0 (Pfeffer et al., 2014; Randolph Glacier Inventory Consortium et al., 2017), with a census date of AD 2005 (Kienholz et al., 2015). They were overlain on Landsat 7 ETM+ satellite imagery of the same date as the source ID attribute in the RGI files, and manually corrected for misclassified snow and ice or lakes. Some glaciers were missing, incorrectly delineated, or had overlapping outlines with other glacier polygons. Lemon Creek Glacier and Taku Glacier were revised to follow published outlines (McNeil et al., 2020).

Glacier outlines were then manually edited according to observed changes around the glacier margin from the 2019 Sentinel satellite

TABLE 2 Sentinel and Landsat imagery used in glaciological and geomorphological mapping

Sensor	Product	Datastrip	Image ID	Date image acquired
Sentinel-2B	S2B_MSIL1C_20190830T201859_N0208_R071_T08VML_20190830T221736	S2B_OPER_MSI_L1C_DS_MTI_20190830T221736_S20190830T202101_N02.08	L1C_T08VML_A012967_20,190,830 T202101	30/08/2019
Sentinel-2B	S2B_MSIL1C_20190906T200939_N0208_R028_T08VNM_20190906T233631	S2B_OPER_MSI_L1C_DS_EPAE_20190906T233631_S20190906T200951_N02.08	L1C_T08VNM_A013067_20,190,906 T200951	06/09/2019
Sentinel-2A	S2A_MSIL1C_20190901T200911_N0208_R028_T08VNL_20190901T233048	S2A_OPER_MSI_L1C_DS_MPS_20190901T233048_S20190901T201750_N02.08	L1C_T08VNL_A021904_20,190,901 T201750	01/09/2019
Sentinel-2A	S2A_MSIL1C_20190907T203011_N0208_R114_T08VML_20190908T001020	S2A_OPER_MSI_L1C_TL_EPAE_20190908T001020_A021990_T08VML_N02.08	L1C_T08VML_A021990_20,190,907 T203043	07/09/2019
Sentinel-2A	S2A_MSIL1C_20190901T200911_N0208_R028_T08VNK_20190901T233048	S2A_OPER_MSI_L1C_DS_MPS_20190901T233048_S20190901T201750_N02.08	L1C_T08VNK_A021904_20,190,901 T201750	01/09/2019
Sentinel-2A	S2A_MSIL1C_20190907T203011_N0208_R114_T08VMM_20190908T001020	S2A_OPER_MSI_L1C_DS_EPAE_20190908T001020_S20190907T203043_N02.08	L1C_T08VMM_A021990_20,190,907 T203043	07/09/2019
Landsat 7 ETM+	LE07_L1TP_058019_20050810_20160924_01_T1			10/08/2005
Landsat 7 ETM+	LE07_L1TP_056019_20050812_20160925_01_T1			12/08/2005

imagery, both in the terminus and forefield, and at higher elevations, to reflect the 2019 AD glacier extent. RGI IDs were maintained for each glacier polygon. Where glaciers had separated into multiple polygons, the same RGI ID was used for both and the glacier was treated as a multipart polygon. Glacier elevation characteristics were derived by comparing mapped 2019 glacier outlines with the composite DEM. Zonal statistics algorithms were applied to compute slope, elevation and aspect data for every glacier.

The higher-resolution Sentinel satellite imagery compared with previous Landsat-based inventories allowed a more detailed glaciological analysis and smaller minimum glacier and lake area of 0.001 km^2 for mapping than earlier inventories (e.g. the glacier inventory of Kienholz et al., 2015). Glaciers were characterized as: (i) outlet glaciers draining from the main icefield, with an interconnected accumulation area; (ii) valley glaciers that flow down the valley with a clearly topographically defined accumulation area; (iii) mountain glaciers adhering to the mountain sides; or (iv) at the smallest scale, glacierets, following RGI and GLIMS protocols (Paul et al., 2009; Rau et al., 2005) (Figure 2). However, we note that the outlet glaciers also occupy the valleys and so may behave in a similar way on their trunks.

Uncertainty in glacier area was calculated following Paul et al. (2013). Eleven representative glaciers, across the spectrum of glacier sizes and including debris-covered and clean-ice glaciers, were digitized seven times, with a minimum of 1 day between each round of digitizing (cf. Paul et al., 2013). The mean, standard deviation (SD) and 95% confidence interval of glacier area was then calculated for each glacier. A regression through the data points (mean glacier area and 95% confidence interval; $r[9] = 0.91$, $p < 0.001$) provided an equation that was used for size-specific up-scaling of the 95% confidence interval to the full dataset, which was used as the uncertainty in glacier area (Paul et al., 2013, 2017; Pfeffer et al., 2014).

Long profiles for glaciers followed the central flowline from the highest to the lowest point on the glacier. They did not cross mapped ice-free areas, longitudinal flowlines or medial moraines, to ensure that they represented single ice-flow units.

Mean glacier slope, aspect and minimum (Z_{min}), maximum (Z_{max}) and median (Z_{med}) elevations for each glacier were derived using zonal statistics using the void-filled ArctciDEM as reference. Glacier hypsometric index (*HI*) was calculated following Jiskoot et al. (2009) and McGrath et al. (2017), where

$$HI = \frac{(Z_{max} - Z_{med})}{(Z_{med} - Z_{min})} \quad (1)$$

But if $0 < HI < 1$, then

$$HI = \frac{-1}{HI} \quad (2)$$

This index is grouped into very top heavy ($HI < -1.5$), top heavy ($-1.5 < HI < -1.2$), equidimensional ($-1.2 < HI < 1.2$), bottom heavy ($1.2 < HI < 1.5$) and very bottom heavy ($HI > 1.5$) glaciers. Top-heavy glaciers have their area distribution strongly skewed towards the top of their elevation range.

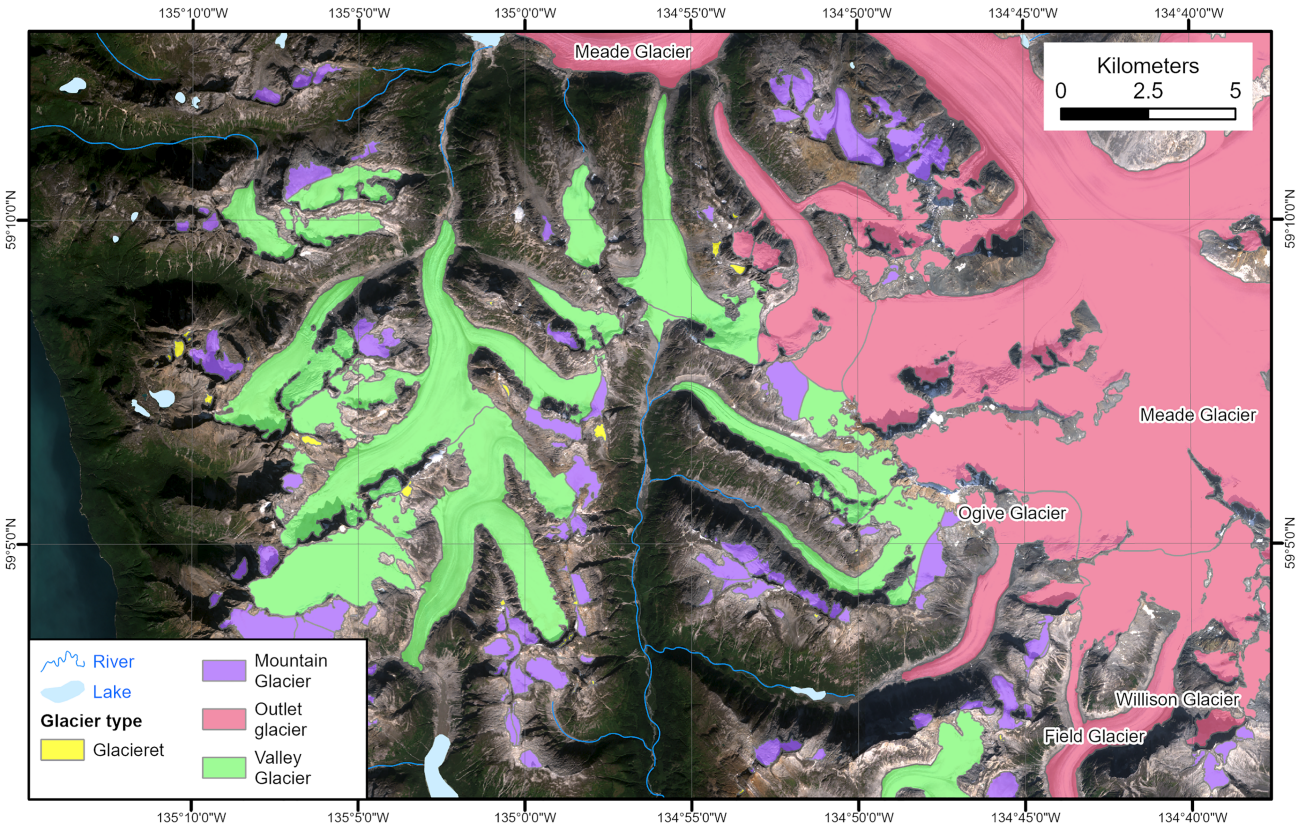


FIGURE 2 Examples of valley glaciers, outlet glaciers, mountain glaciers and glacierets on and around Juneau Icefield. [Color figure can be viewed at wileyonlinelibrary.com]

2.3 | Glacier lakes

Lakes were manually digitized using the Sentinel imagery and were categorized as ice-contact proglacial, ice-dammed, supraglacial and ice-distal. Supraglacial lakes were visible as a dark-blue area with well-defined boundaries on the glacier surface. Ice-dammed lakes were visible as a marked flat area with clear boundaries on the DEM. They were visible on the Sentinel imagery as either a blue lake with numerous calved icebergs, or as a recently drained lake demarcated by shorelines, flat-topped glaciolacustrine sediments and chaotic iceberg remnants (Figures 3a–c). The highest shoreline was used in lake demarcation. The calving terminus of these lakes is often associated with a zone of intense concentric to half-oval crevassing, and a depression in the ice (cf. Stone, 1963). This was mapped, for example, on Gilkey Glacier (Figure 3b), and was used to help identify locations of ice-dammed lakes. Ice-dammed lakes were mapped to show maximum recent extent, as they are often drained in August, the date of the satellite imagery (Geertsema & Clague, 2005; Kienholz et al., 2020). Ice-dammed lakes were therefore cross-checked against the ArcticDEM and higher-resolution ESRI Basemap imagery of a different date to ensure correct identification.

Ice-contact proglacial lakes in direct contact with the glacier terminus ranged from large lakes with calved icebergs (Figure 3d) to small tarns in the base of cirques. These lakes form in the overdeepening in front of the glacier margin and are dammed by either moraine or bedrock. Moraine-dammed lakes were identified by the presence of a clearly defined ridge across the drainage point for the lake (Figure 3e).

2.4 | Glacier structures

The plateau area on the main icefield is mapped where the ice is interconnected without topographical barriers, the ice surface slope is <10° and the elevation is >1200 or 1500 m a.s.l. Two-dimensional structures across the icefield were traced and digitized as ESRI Shapefiles from the Sentinel-2 satellite imagery (Table 2). Structural features were identified using standard criteria (Cuffey & Paterson, 2010; Goodsell, Hambrey, & Glasser, 2005; Goodsell, Hambrey, Glasser, Nienow, et al., 2005; Hambrey & Lawson, 2000; Jennings et al., 2014, 2016) (Table 3). Features mapped included primary structures related to the accretion and deposition of snowfall (e.g. primary stratification) and brittle (crevasses) or ductile (foliation, ogives and longitudinal flow stripes) secondary structures related to deformation (Colgan et al., 2016; Hambrey, 1994; Kellerer-Pirklbauer & Kulmer, 2019). A single point is mapped for icefall-type crevasses occurring together in one ice-flow unit, allowing the number of icefalls to be calculated. Other features mapped include rock glaciers, supraglacial debris cover, medial moraines and debris flows (Table 3).

Mapping was focused on the ablation portions of the glaciers. Snow-covered structures in the accumulation areas of the glaciers may therefore be under-mapped. The values given in this dataset should thus be considered minimum values. The resolution of the satellite imagery used also makes it difficult to observe smaller crevasses or features such as moulins and supraglacial channels. The resultant dataset is designed to be viewed at up to 1:10 000 scale.

Glacier 'disconnections' occur where lower portions of the glacier become discontinuous with higher elevation areas, which formerly

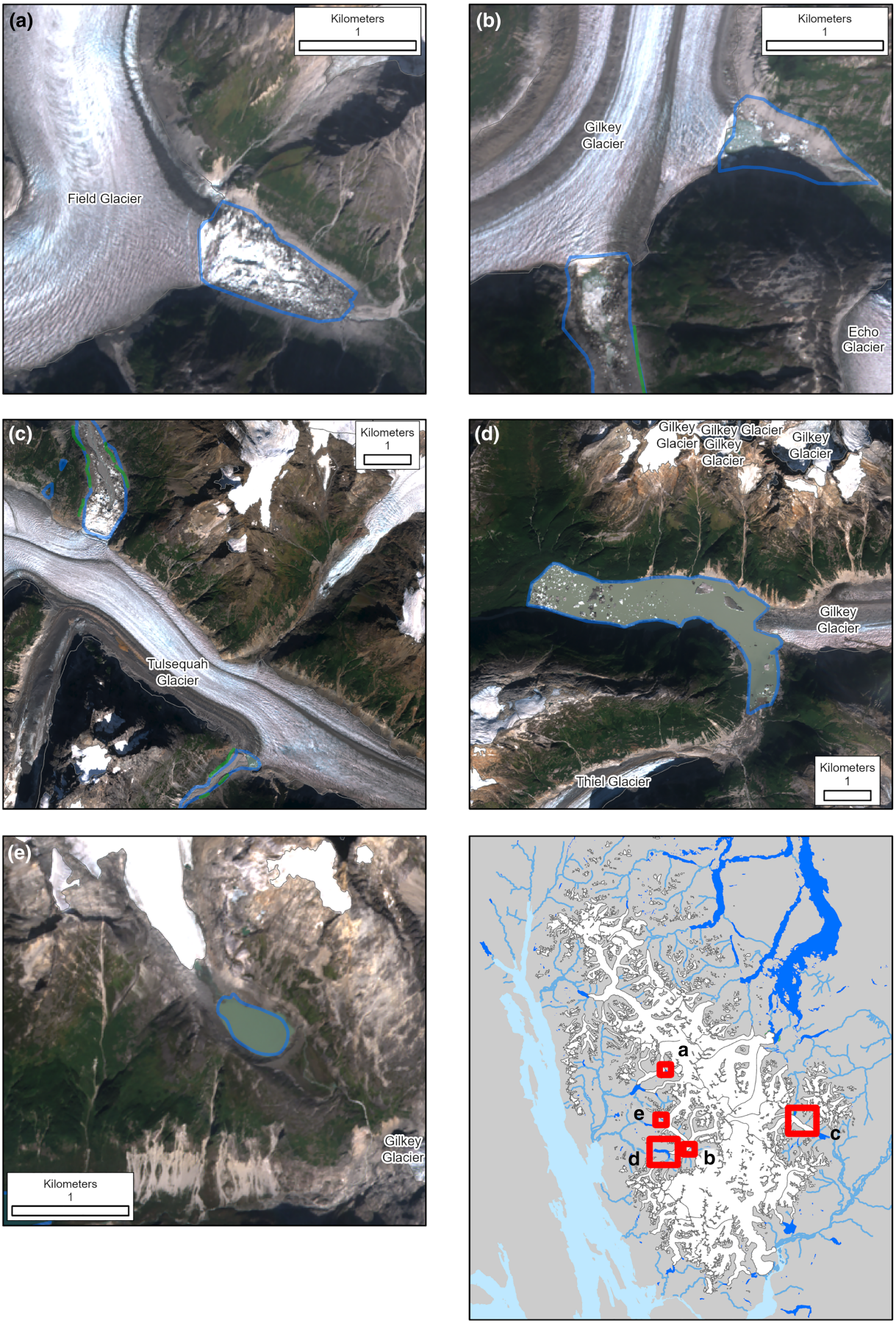


FIGURE 3 Examples of ice-marginal lakes, including proglacial ice-dammed (a–c), proglacial bedrock-dammed (d) and an ice-distal moraine-dammed lake (e). Lakes are outlined in blue. [Color figure can be viewed at wileyonlinelibrary.com]

TABLE 3 Summary of structures from satellite imagery, including their spatial distribution across Juneau Icefield

Structure	Identification on satellite imagery	Proposed mechanism of origin	Location on glaciers of Juneau Icefield
Snowline	Wavy, discontinuous boundary between bright white and duller blue-grey.	Higher albedo snow reflects a brighter white colour.	Accumulation zone. Features above this are largely snow-covered.
Primary stratification	Continuous, wavy, transverse layers, parallel to equilibrium line. Layering becomes folded down-glacier.	Firnification processes in accumulation area producing original layering (Hambrey & Clarke, 2019; Jennings et al., 2016).	Upper, accumulation parts of glaciers on Juneau Icefield.
Folded primary stratification	Darker and whiter layers showing deformation and folding, with fold axes parallel to inferred flow.	Attenuation, folding and deformation of primary stratification by ice flow (Lovell et al., 2015).	Down-ice of primary stratification, showing increased attenuation with distance. Found mostly on trunk of valley glaciers.
Longitudinal foliation/ flowlines	Long, linear traces, parallel to ice flow.	Increased attenuation and folding of folded primary stratification; transposed pre-existing layering eventually leading to isoclinal limbs parallel to ice flow (Hambrey & Clarke, 2019). Folding along the axial plane of medial moraines and primary stratification may be indicative of past surging activity (Copland et al., 2003; Evans & Rea, 2003; Grant et al., 2009).	Trunks of valley glaciers in areas of convergent flow. Define flow units. Form especially where multiple accumulation basins combine in one trunk, forcing lateral compression of the glacier.
Transverse crevasses	Short to long traces transverse to flow. Occur within a single flow unit. Visible as straight, dark lines on satellite imagery.	Crevasses are open fractures in the ice, caused by brittle deformation in response to stress (Colgan et al., 2016). They form due to extensional flow in the glacier, where extending flow produces a tension that is transverse to flow.	Form across glacier where extensional flow is significant. In the upper parts of the glacier, extending flow forms transverse crevasses extending arcuate up-glacier across the entire width.
Marginal crevasses	Short traces at the valley side, angled obliquely to ice flow. Often arc up-ice at ~45°. Typically within a single flow unit.	Form at lateral margin of glacier due to shear against valley sides (Jennings & Hambrey, 2021; Jennings et al., 2014; Jiskoot et al., 2017).	Common on the trunks of valley glaciers, against valley side, especially around the edge of the plateau.
Icefalls	Extensional, arcuate transverse crevasses at the top of a region of intense, chaotic, densely crevassing with a steep ice-surface slope. Often have ogives/ Forbes Bands forming beneath. Associated with a change or increase in glacier steepness.	Form due to brittle fracture where the glacier flows over a region of increased steepness. Indicative of a compressive flow regime (Jiskoot et al., 2017).	Common in steep areas on outlet glaciers draining the main icefield, valley glaciers and mountain glaciers.
Ogives	Arcuate structures with dark and light bands located below icefalls. Also known as Forbes Bands.	Represents ice flow through an ice fall, with a darker and a lighter band each year (Jennings & Hambrey, 2021; Jiskoot et al., 2017). Form annually as bulge waves due to a seasonal acceleration of the ice through an icefall. The acceleration is exacerbated in horizontally restricted icefalls. They then form a series of arcuate wave crests and troughs, pointing down-glacier. They gradually flatten until they are left as arcuate bands of lighter and darker ice on the surface of the glacier; the darker bands are the dense, blue, dusty ice that is compressed in summer and the white bands are the bubbly, air-filled ice that is compressed in winter.	Downstream of icefalls on the trunks of valley and outlet glaciers.

(Continues)

TABLE 3 (Continued)

Structure	Identification on satellite imagery	Proposed mechanism of origin	Location on glaciers of Juneau Icefield
Longitudinal and splaying crevasses	Linear (along-flow) to radial traces.	Longitudinal crevasses form where valley glaciers are able to spread laterally due to a turn or a widening in the valley. Splaying crevasses form in the terminus of glaciers, where the glacier enters a region less topographically confined and is able to spread laterally.	Longitudinal crevasses form on the trunk of valley glaciers where the valley widens or where the valley makes a turn. Longitudinal crevasses form under strong compression. Splaying crevasses are found mostly at the terminus of piedmont lobe, land-terminating glaciers.
Rifts	Broad, open crevasse at terminus of the glacier, which penetrates the entire depth of the floating terminus of a glacier. Lake water (frozen or melted) may be visible within the rift.	Associated with terminus flotation, extension and calving.	Glacier terminus where ice ends in proglacial lake.
Iceberg	Bright white, dull grey or brown feature within a proglacial ice-contact lake.	Indicates calving activity of the glacier.	Glacier terminus where ice ends in a substantial lake with calving forming part of glacier ablation.
Medial moraines	Dark brown to black in colour. Long linear traces emanating from point sources, usually at the junction where two tributary basins meet.	Supraglacial debris falling onto ice surface and being transported down-ice by ice flow at the junction of two tributary glaciers.	Trunks of valley glaciers or outlet glaciers, in the ablation zone.
Debris flows	Dark brown to black in colour. Rough surface texture in appearance. Lobate form. Origin from valley sides or glacier headwall.	Represents rock avalanches or debris flows onto the glacier surface. An important mechanism for inputting supraglacial debris into the system.	Trunks of valley glaciers or outlet glaciers, or near the top of the glacier at the headwall.
Debris cover	Smooth texture, dark grey in colour, frequently emanating from sources on valley sides.	Dust blowing onto glacier surface; supraglacial debris falling onto glacier surface; ablation of glacier transferring debris to the surface.	Ablation zone of glaciers.
Glacier disconnection	Dark or grey-coloured bedrock visible within the glacier polygon, separating accumulation and ablation areas of the glacier. They are mapped where recession and icefield fragmentation has resulted in a disconnection between the glacier tongue and its accumulation area. This is visible in the 2005 to 2019 satellite imagery or in the mapped glaciology and geomorphology, which shows an older connection between contiguous ice units. As such, glacier disconnections are mapped that occurred between the LIA and the present day.	Thinner, heavily crevassed ice with steep ice-surface slope occurs over bedrock steps or areas of steep bedrock. The thinner ice here ablates, leading to the emergence of bedrock within the glacier polygon. An aspect of fragmentation of the icefield during glacier recession.	Associated with icefalls or steep, heavily crevassed terrain (e.g. Figure 4).
Glacier separation	Dark grey-coloured bedrock visible between a tributary and trunk glacier on valley floor. Separations are identified where glacier recession between 2005 and 2019 exposes bedrock between tributaries, or where glacial geomorphology or flowlines within the ice indicate an earlier separation (e.g. contiguous moraines indicate a previously confluent tributary is now separated). Separations are therefore mapped between the LIA and the present day.	Associated with recession of a tributary glacier from a trunk outlet or valley glacier, resulting in two or more discrete glacier termini.	Associated with recession and increasing fragmentation of glaciers; found in valley floors or on valley walls, where glaciers shrink laterally as well as along their length (e.g. Figure 4).

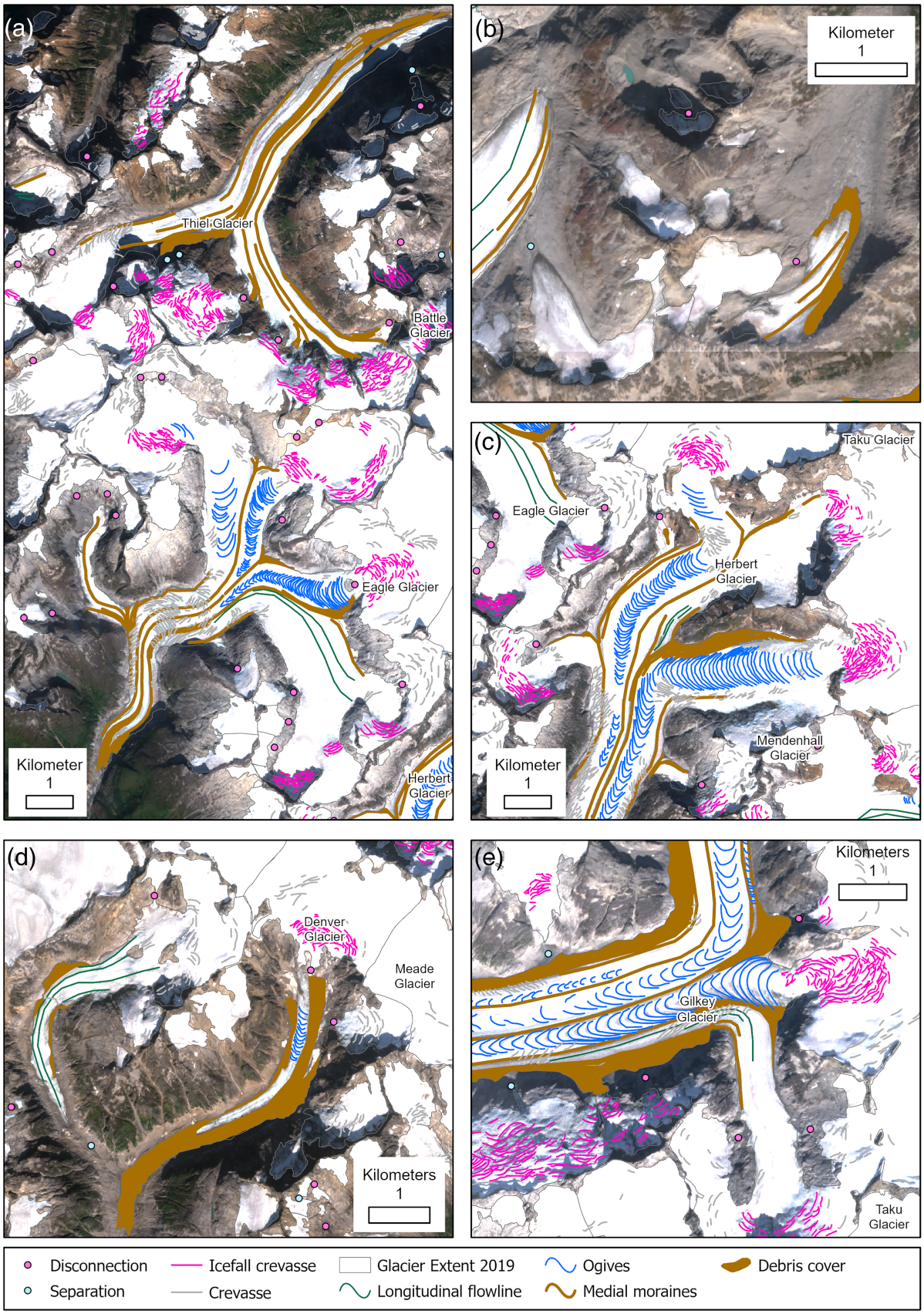


FIGURE 4 Examples of glacier disconnections and separations across Juneau Icefield. (a) Eagle and Thiel glaciers. (b) Examples of mountain glaciers and small valley glaciers. (c) Herbert Glacier. (d) Denver Glacier. (e) Gilkey Glacier, showing Vaughan Lewis and Little Vaughan Lewis icefalls (disconnected). [Color figure can be viewed at wileyonlinelibrary.com]

supplied ice (Boston & Lukas, 2019; Jiskoot et al., 2009; Rippin et al., 2020). They are typically found in icefalls or steep, heavily crevassed areas (Table 3; Figure 4). Disconnections are mapped here where a glacier flow unit, defined by mapped longitudinal flowlines or medial moraines, has become disconnected from higher-elevation areas and can no longer receive nourishment down-glacier, with bare

rock visible. Although the term 'detachment' has previously been used (Rippin et al., 2020), this term has also been used in relation to catastrophic failures of mountain glaciers as they become detached from their bedrock (e.g. Jacquemart et al., 2020), and so 'disconnection' is preferred here.

Glacier disconnections are mapped where they are visible in the disconnection of glacier outlines between the 2005 and 2019 censuses, and also where structural glaciology (e.g. flowlines, medial moraines, foliation) and geomorphology (e.g. moraines, trimlines, flutes, bedrock lineations) are indicative of formerly confluent ice flow (e.g. on Eagle Glacier; Figure 4b). As such, all mapped disconnections occurred between the LIA neoglaciation and 2019.

Glacier disconnections differ from reconstituted glaciers (Benn & Lehmkuhl, 2000), which derive inflow of snow and ice via avalanching processes, and so still receive mass inflow from their accumulation area, even though unglaciated rock slopes up to several hundred metres high may divide the glacier. Reconstituted glaciers form below a hanging glacier, and near-vertical slopes are required for this. The glacier disconnections observed in this study typically occur on shallower slopes where ice-avalanching processes are less common. Where we have mapped disconnections, we see no evidence of accumulation through ice avalanching.

A second example of icefield fragmentation is 'separation', where tributary glaciers have receded from a trunk glacier (Figure 4). They are common in valley floors as the glaciers recede, resulting in discrete glacier termini. They also occur on mountain sides, where lateral shrinkage has resulted in multipart polygons in our inventory. However, these tributary separations do not occur over bedrock steps, and do not separate accumulation and ablation areas. They are identified both where they are visible in the separation of glacier outlines between 2005 and 2019, and also where mapped geomorphology (e.g. moraines, trimlines, flutes) or structural glaciology (e.g. flowlines, foliation, medial moraines) is indicative of formerly confluent tributaries. As such, all mapped separations occurred between the LIA neoglaciation and 2019.

2.5 | Glacial geomorphology

Glacial landforms were mapped following standard remote sensing protocols using the Sentinel-2 satellite imagery and the hillshade of the composite 2 m ArcticDEM. Mapping was conducted at a range of scales, producing a dataset designed at 1:10 000 scale. Again, this leads to a bias towards mapping larger and more prominent features. Areas in shadow and heavily vegetated older moraines may also be under-mapped. The features presented in this dataset should therefore be considered a minimum. Features of all ages were mapped.

Identification of glacial landforms from satellite imagery has been well established (Bendle et al., 2017; Benn & Evans, 2010; Chandler et al., 2018; Darvill et al., 2017; Glasser et al., 2005, 2008; Martin et al., 2019). Identification criteria from Table 1 of Martin et al. (2019) were principally applied, with a focus on subglacial and ice-marginal landforms. All landforms, of all ages, that were clearly visible in the satellite imagery were mapped.

The well-defined, sharp-crested moraines and composite moraines that surround the forefields of most glaciers are assumed to date from the LIA maximum (with the exception of Taku Glacier). They form a clear and decisive marker around the ice-scoured bedrock, diamicton or fluted till found within the glacier forefields. Fluted till presents as a series of closely spaced, regular, small-scale ridges, which distinguishes it from the larger and more singular moraine ridges. Morphostratigraphic principles (Boston et al., 2015; Lukas, 2006; Lüthgens & Böse, 2012) were applied to differentiate between the LIA neoglacial moraines and older, more degraded moraines deposited in the Younger Dryas or earlier Holocene glaciations. In most cases, Holocene neoglaciations are likely to have been smaller than, and within the limits of, the LIA (Barclay et al., 2009; Clague et al., 2010; Koch & Clague, 2011), which makes confusion of ice limits less likely. This is supported by published work reconstructing the LIA around Juneau Icefield (Table 1).

3 | GLACIOLOGICAL INVENTORY AND STRUCTURAL MAPPING

3.1 | Glacier inventory

3.1.1 | Glacier area

The original RGI dataset included 1193 glaciers, with a total area of 4238.5 km^2. The corrected and updated RGI 2005 files comprised 1113 glaciers, with a total area of 4238.7 $\pm$ 47.6 km^2. Mean glacier area was 3.8 km^2 (SD 26.5), with a median area of 0.41 km^2. Individual glacier area ranged from 0.012 to 736.07 $\pm$ 2.39 km^2.

In 2019 AD, the study area comprised 1050 glaciers (Table 4) with a mean area of 3.60 km^2 (SD 26.3), a median area of 0.27 km^2 and a total area of 3816.43 $\pm$ 15.92 km^2. Individual glaciers ranged from 728.60 $\pm$ 0.96 to 0.002 km^2. Over the 14-year time difference between the two surveys (2005 and 2019), 63 glaciers disappeared, and there was a reduction in glacier area of 422.3 km^2 (10.0%), at a mean rate of 30.16 km^2 a^{-1}.

The contiguous area of Juneau Icefield, including small glaciers within the icefield boundaries, comprises 218 glaciers (36 glacierets,

TABLE 4 Count and descriptive statistics for Juneau Icefield in 2019 AD

Glacier type	Count	Total glacier area (km^2)	Total area uncertainty (km^2)	Number of lacustrine-terminating glaciers	Mean median slope (°)	Mean Z_{med} (m)	Mean area (km^2)
Glacieret	281	27.2	3.0	8	23.6	1593.7	0.1
Mountain glacier	584	279.2	6.4	15	19.5	1529.7	0.5
Valley glacier	145	570.9	2.3	6	13.9	1562.3	3.9
Outlet glacier	40	2939.1	4.2	12	10.9	1490.3	73.5
Total	**1050**	**3816.4**	**15.9**	**41**	**19.5**	**1549.8**	**3.6**

108 mountain glaciers, 34 valley glaciers and 40 outlet glaciers). Together, these glaciers covered a total area of 3251.3 ± 6.5 km^2 in 2019. Glacier area in 2019 was strongly skewed; 66% of the glaciers within the region were less than 0.5 km^2 in size, yet only represent 3% of the area (119.6 ± 7.4 km^2; Figure 5a). The 40 icefield outlet glaciers in contrast cover 2939.1 ± 4.2 km^2 (77%; Figure 5b). Outlet glaciers descend from the high, low-slope interconnected plateau to the confined valleys. They largely have a tributary form, with multiple accumulation basins joining together to form one main trunk in one valley with strongly convergent flow. The largest outlet glacier is Taku Glacier (728.6 ± 1.0 km^2). Meade Glacier is the second-largest; it covered 423.8 ± 0.6 km^2 in 2019 and calved into a proglacial lake (4.7 km^2). On the other side of the icefield, the third largest is Llewellyn Glacier (290.8 ± 0.4 km^2 in 2019; calving into a proglacial lake [11.9 km^2] at 725 m a.s.l.).

The study area includes 145 valley glaciers (e.g. Figure 2), 584 mountain glaciers and 281 glacierets (Table 4; Figure 5b). The aspect of the outlet glaciers is mostly west–east, reflecting the central ice divide along the icefield, but the peripheral small mountain and valley glaciers have a predominantly northerly aspect (Figures 5c and d). Glacier maximum elevation is 773 to 2496 m, with a mean of 1747.1 m a.s.l.

There was little discernible difference in mean Z_{med} between glacierets, mountain glaciers and valley glaciers (1529–1593 m a.s.l.), or in the different aspect zones (Figures 5e and g). Z_{med} was normally distributed, ranging from 694 to 2186 m a.s.l. (Figure 5f).

Glacier median slope ranged from 2.5 to 60.1° (Figure 5h), with glacierets and mountain glaciers having a higher average median slope than outlet glaciers (Table 4; Figure 5i). The plateau area has a slope typically of 3–5°. Some glaciers show a stepped profile owing to steep (>30°) icefalls that connect the low-slope accumulation (<5°) and ablation zones (<10°) (e.g. on East Twin, West Twin, Tulsequah, Gilkey, Battle and Field glaciers; Figure 6).

3.1.2 | Glacier hypsometry

The Juneau Icefield outlet glaciers were dominantly top heavy or very top heavy (Table 5). Of the total 3816.4 km^2 of glacier area in the study area, 1993.8 km^2 was very top heavy, with 857.7 km^2 being top heavy. The smaller valley and mountain glaciers and glacierets were more evenly spread across the hypsometric categories, but equidimensional glaciers were the most numerous. Bottom-heavy glaciers account for only a small fraction of the glacier area in the Juneau Icefield region (Table 5). Whilst equidimensional glaciers were most numerous here, this is due to the smaller mountain and valley glaciers fringing the icefield, whilst the icefield has a small number of very top-heavy outlet glaciers that contain the majority of the glacier area.

3.1.3 | Rock glaciers

Ten rock glaciers were mapped, typically backed onto steep cliffs that provided the required talus input. Individual rock glaciers ranged from 0.04 to 0.94 km^2, with a total area of 3.2 km^2. They were observed around the fringes of the icefield region, especially to the north, where glacierets and smaller mountain glaciers are most prevalent (Figure 7). However, the 10 m resolution of the Sentinel imagery challenged the differentiation of these small features from moraines.

3.2 | Glacial lakes

We mapped 368 lakes, including 23 supraglacial, 28 ice-dammed, 47 proglacial ice-contact, 38 tarns in cirque basins and 232 ice-distal lakes (Table 6; see examples in Figure 3). These numbers include seven moraine-dammed lakes: the proglacial lake in front of East and West Twin glaciers, one ice-distal lake in a tarn (Figure 3e) and four small proglacial ice-contact lakes in front of cut 'two' mountain glaciers (Table 6). Twelve outlet glaciers terminated in proglacial lakes, which ranged from 12.6 km^2 (East and West Twin Glacier) to 1.5 km^2 in size. The remaining proglacial lakes were all smaller than 0.5 km^2, and were mostly associated with over-deepenings in the base of cirques. In total, the ice-contact proglacial lakes of Juneau Icefield covered 58.4 km^2, with most of the water volume in the above listed lakes associated with outlet glaciers. Calving is apparent as some of the larger proglacial lakes contain icebergs (e.g. in front of Field, Tulsequah, Meade, Llewellyn, Norris and Gilkey glaciers). Most glacier termini appear to be grounded, although limited rifting and extensive longitudinal and splaying crevassing in Norris, Meade and Field glacier termini suggests at least partial flotation. Field Glacier has a number of large tabular icebergs within its lake, which have calved from the ice margin, which also suggests at least partial flotation. Rifts elsewhere are rare, likely because the majority of glaciers remain grounded in their relatively shallow proglacial lakes, with limited flotation in the centre of the ice terminus. Small ice-contact moats with minor icebergs are now present at the terminus of Taku Glacier, and at its northern branch, Hole-in-the-Wall Glacier. The remaining outlet glaciers terminate on land, most frequently on ice-scoured bedrock. The remaining outlet glaciers terminate on land, most frequently on ice-scoured bedrock. The vast majority of the smaller mountain glaciers of Juneau Icefield are land-terminating (Tables 4 and 6; Figure 7).

Many of the larger outlet glaciers are also associated with marginal ice-dammed lakes (Table 6; Figure 3). As glaciers recede from side valleys and tributaries separate from the main glacier trunks since the LIA neoglacial maximum, lakes are forming and draining subglacially towards the ice margin. Ice-dammed lakes were mapped adjacent to Field, Meade, Mendenhall, Gilkey, Llewellyn, Norris, Hole-in-the-Wall, West Twin, Taku and Tulsequah glaciers. The 28 mapped ice-dammed lakes is an increase on the 10 lakes listed in previous studies (Stone, 1963). A small number of supraglacial lakes were observed on Norris, Taku and Field glaciers.

In several places, proglacial rivers in tributary valleys can be seen to disappear under larger glaciers, presumably flowing subglacially rather than around the lateral margins (e.g. under Tulsequah and Meade glaciers).

3.3 | Structural glaciological mapping

Here, we present the first structural glaciological map for an Alaskan icefield (Figures 7 and 8; Table 7). This new database includes 20 809 individual structures, with elevation data, including 16 358 crevasses in 2387 heavily crevassed zones, evidence of ductile

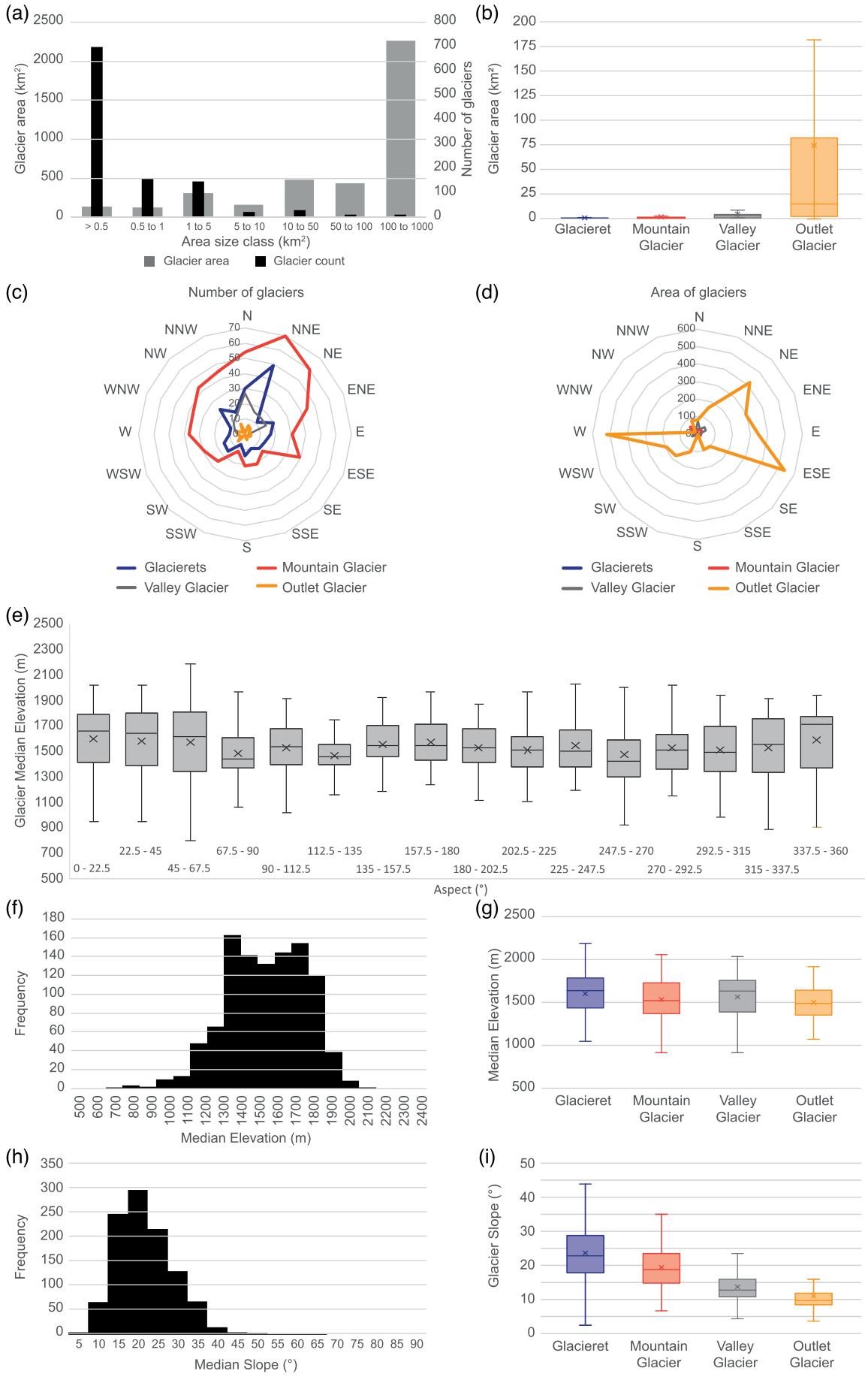


FIGURE 5 Legend on next page.

FIGURE 5 Descriptive statistics for glaciers in Juneau Icefield in 2019 AD. (a) Bar chart showing number and area of glaciers. (b) Box and whisker plot for glacier area for different classifications of glaciers. (c) Radar plot of glacier aspect with glacier number. (d) Radar plot of glacier aspect with glacier area. (e) Box plots of glacier median elevation in different aspect zones. (f) Histogram of glacier median elevation. (g) Box plots of glacier median elevation for different glacier classifications. (h) Histogram of glacier median slope. (i) Box and whisker plot of glacier slope with different glacier classifications. [Color figure can be viewed at wileyonlinelibrary.com]

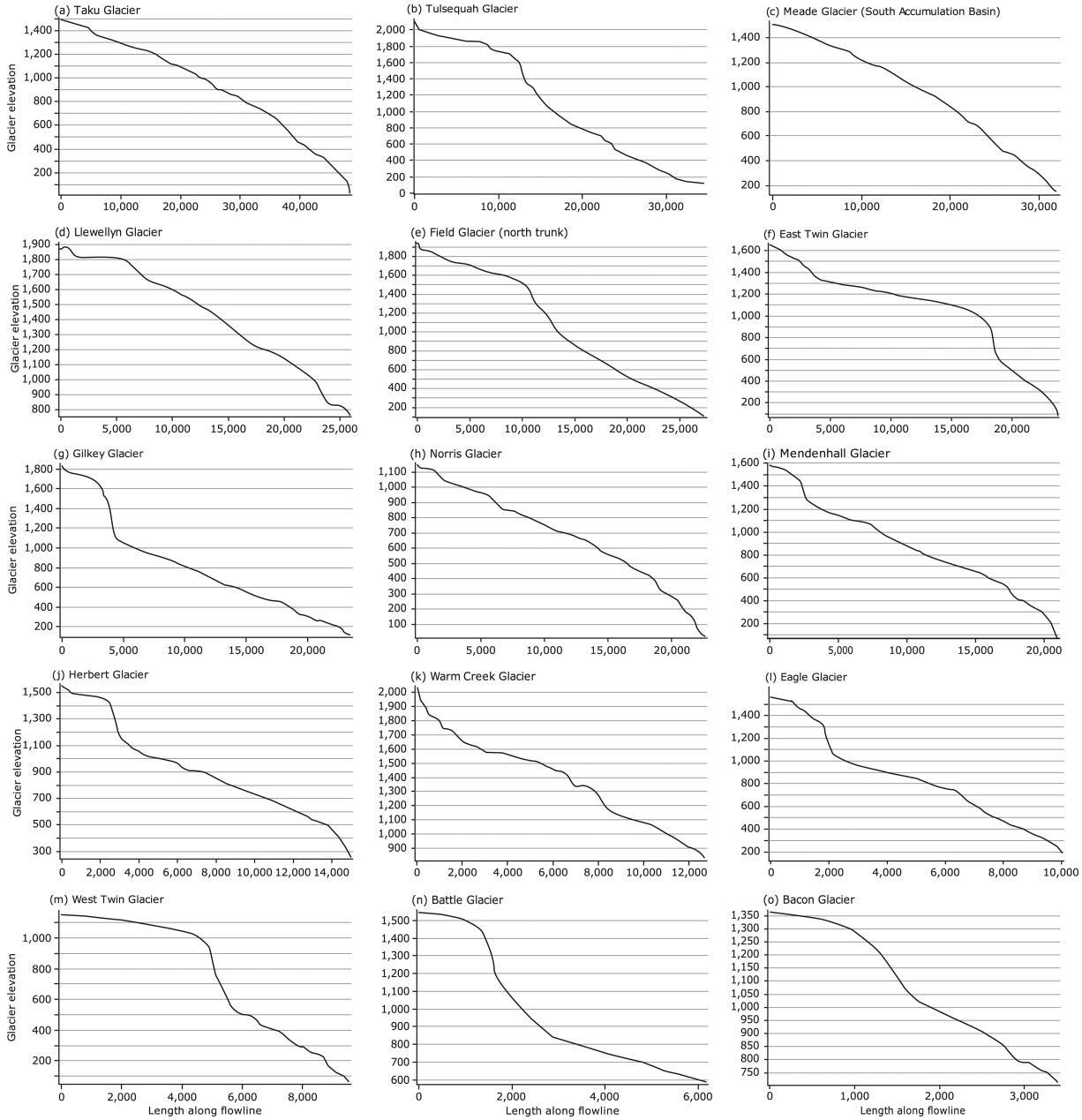


FIGURE 6 Long profiles of ice surface down centreline of key outlet glaciers of Juneau Icefield. Glacier profiles were derived from ASTER GDEM along the centre flowline. Profiles are organized sequentially from the longest (a) to the shortest (o) glacier. Note that *x* and *y* axes are not comparable. Length and elevation in metres (m).

deformation in the form of deformed foliation and ogives, and limited supraglacial debris cover.

3.3.1 | Foliation and primary stratification

Primary stratification (Hambrey & Clarke, 2019; Jennings et al., 2014) (Table 3) is common in the higher parts of the glaciers. Down the glacier trunk, it is progressively attenuated, deformed and folded. This large-scale, asymmetric folding occurs around flow-parallel fold axes, and occurs within flow-unit boundaries. Continued folding eventually leads to long isoclinal limbs, parallel to ice flow (Lovell et al., 2015). These longitudinal planar structures (longitudinal foliation) are particularly well developed where several accumulation basins are tributaries to one key trunk. Clear examples are observed on Meade (Figure 9), Llewellyn, Gilkey (Figure 10) and Taku glaciers.

Longitudinal foliation structures are oriented parallel to ice flow, and clearly demarcate flow-unit boundaries. They form in areas of converging flow, where simple shear and longitudinal extension dominate (Hambrey, 1977; Hambrey & Lawson, 2000; Jennings

TABLE 5 Summary of glacier hypsometry; count of glaciers is provided

Glacier type	Count	Very bottom heavy (*HI* > 1.5)	Bottom heavy (1.2 < *HI* < 1.5)	Equidimensional (−1.2 < *HI* < 1.2)	Top heavy (−1.5 < *HI* < −1.2)	Very top heavy (*HI* < −1.5)
Outlet glacier	40	1	1	15	10	13
Valley glacier	145	38	26	43	19	19
Mountain glacier	584	109	88	188	99	100
Glacieret	281	42	38	92	54	55
All glaciers	**1050**	**190**	**153**	**338**	**182**	**187**
Glacier area (km^2)	3816.4	185.1	127.5	652.3	857.7	1993.8

et al., 2014). They form parallel to medial moraines and separate out crevasse domains in different flow units. On Meade Glacier, the deformed foliation in the upper reaches of the glacier links clearly to the longitudinal flowlines observed on the main trunk (Figure 9). On dead-ice portions of glaciers, deformed primary stratification helps to identify areas of ice with limited ice flow or contribution to the main glacier trunk. This phenomenon is visible on Dead Branch of Norris Glacier. Larger-scale fold structures, with the axial plane parallel to the ice margin, are apparent on Gilkey Glacier (Figure 10). The looped longitudinal foliation and medial moraines on the northern tributary of the glacier are characteristic of prior surging activity.

3.3.2 | Crevasses

In total, 16 358 crevasses of different kinds were mapped and ascribed to different categories (Table 7). Bergschrunds form at the highest elevation (Figure 8a), at the head of the glacier, where glacier flow causes detachment from the rock wall at the head of the cirque. Heavily crevassed zones were observed on the trunks of many outlet glaciers, including Taku, Meade (Figure 9), Gilkey (Figure 10), Llewellyn, Tulsequah (Figure 11), Field and Mendenhall glaciers (Figure 12).

Transverse crevasses were observed on 199 glaciers. They were mainly found on the trunks of valley glaciers, outlet glaciers and on the steeper mountain glaciers. Transverse crevasses typically formed in clear domains in single flow units, well demarcated by longitudinal flow structures and medial moraines (e.g. Figure 9). These transverse crevasses are frequently observed in the upper parts of the glacier, where extensional flow dominates (Table 3). They also form where an increase in steepness along the longitudinal profile of the glacier encourages extensional flow. This results in a large altitudinal range for this crevasse type (Figure 8a). The steep slopes of the mountain glaciers encourage frequent formation of transverse crevasses. Finally, transverse crevasses oriented in a zone of concentric to oval crevassing were observed at the lateral margins of valley glacier trunks in association with ice-dammed lakes (Figure 3).

Marginal crevasses (Table 3) are common on the trunk of valley glaciers and outlet glaciers. On Mendenhall Glacier (Figures 12 and 14), the marginal fractures become increasingly angled up-glacier, further down the glacier trunk.

3.3.3 | Icefalls and ogives

Icefalls (Table 3) were observed on 23 outlet glaciers, including on 13 outlet glaciers draining down from the main interconnected plateau (Figures 9–14). They are also common on peripheral valley and mountain glaciers. In total, 4981 icefall-type crevasses were mapped, equating to 150 icefalls observed on 55 glaciers. The mean elevation of the icefall-type crevasses is 1481 m a.s.l. (SD 212), with a range of 810 to 2121 m (Table 7; Figures 8a and f). The elevation of the icefall-type crevasses is normally distributed (Figure 8c).

On 11 outlet and 2 valley glaciers, ogives (Table 3) were observed below the icefalls (note their lower mean altitude in Figure 8a); these included Gilkey (Figures 10 and 14), Battle, Denver, West Twin and East Twin (Figure 13), Tulsequah, Field and Bacon glaciers. These ogives largely remain perpendicular to ice flow and remain confined to single flow units (e.g. Figures 11 and 14). They typically become increasingly oriented oblique to ice flow further down the main trunk, as compressive forces become more dominant.

3.3.4 | Splaying and longitudinal crevasses

Llewellyn and Taku are piedmont lobe glaciers characterized by splaying crevasses at their snout (Figures 13 and 14f), caused by ice spreading laterally as it slows and reaches the unconfined, flat valley floor. Most other outlet glaciers terminate in a constrained glacial valley, and therefore lack splaying crevasses at the terminus.

Longitudinal crevasses form in places on the glacier tongue with extensional flow, and where the valley becomes wider, allowing the glaciers to extend laterally as well as horizontally. They typically form lower down the glacier (Figure 8a). Clear examples are observed on West Twin Glacier (Figure 13). They also form at the terminus of some lacustrine-terminating glaciers, such as Mendenhall (Figure 12).

3.3.5 | Debris cover and medial moraines

Surficial debris cover was identified on 111 (10.6%) glaciers, with a maximum area on Gilkey Glacier of 14.4 km^2 (6.5% of its area) (Figure 15). The total debris-covered area was 72.9 km^2 (2.1% of all glacier area). Debris was predominantly found in a thin, superficial covering over the glacier surface, concentrated towards the lateral and terminal margins of the glaciers. The percentage of individual glacier area covered with debris ranges from 0.13% (RGI60–01.00709; 103.31 km^2) to 74.35% (RGI60–01.00731; 0.26 km^2). Glacier size was the overwhelming control on percentage of debris cover; all glaciers with >10% debris cover were under 10 km^2.

Of the glaciers with debris cover, 22 were outlet glaciers, 52 were valley glaciers, 30 were mountain glaciers and 7 were glacierets (Figure 15). However, of these, the percentage of debris-covered area

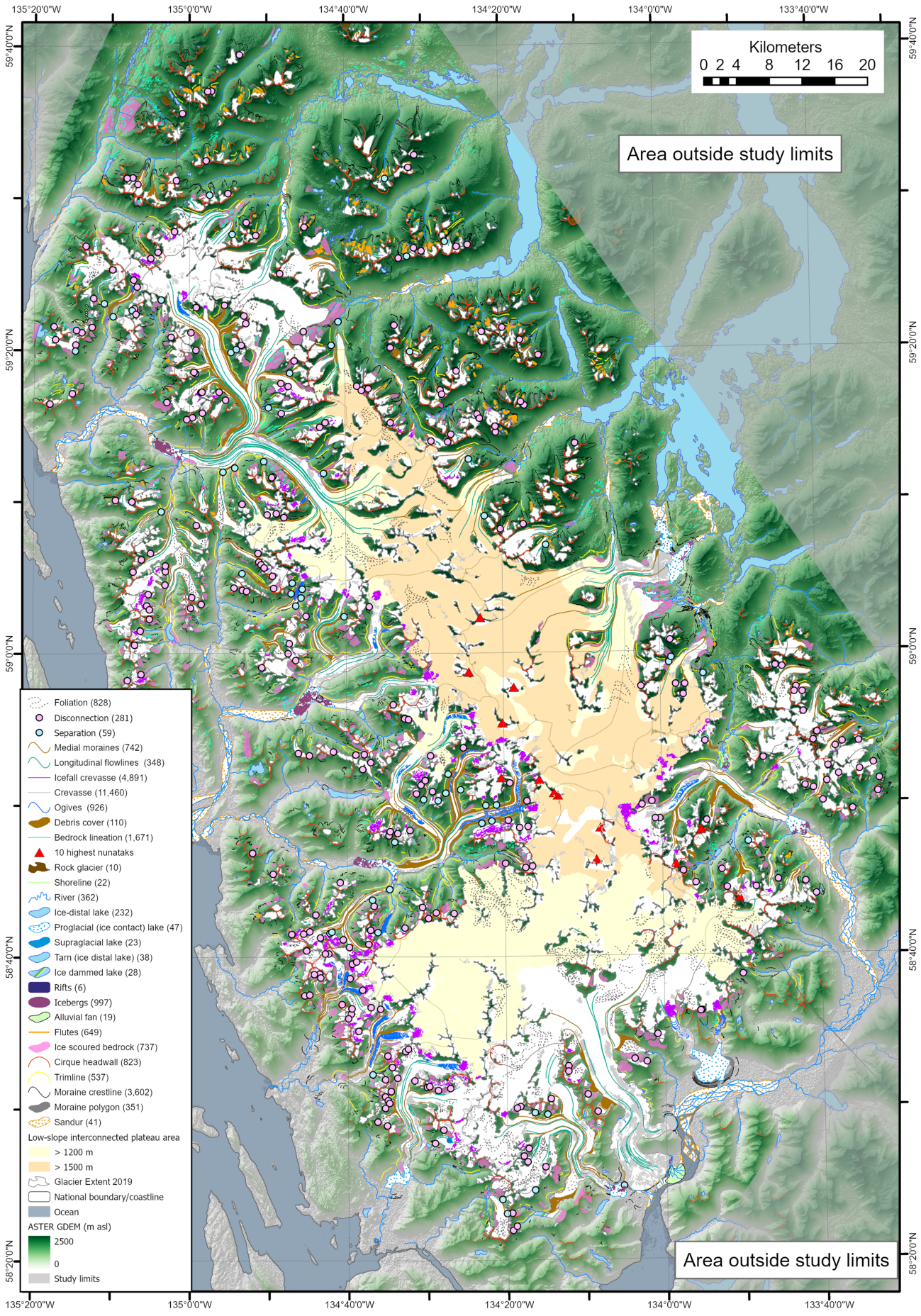


FIGURE 7 Geomorphological and glaciological map of Juneau Icefield in 2019, with number of observations in brackets in the legend. This figure is also available as an A0 map in the online Supplementary Information along with ESRI Shapefiles. Overlain on hillshaded ASTER GDEM. [Color figure can be viewed at wileyonlinelibrary.com]

TABLE 6 Count of different types of lake in the study area. *Moraine-dammed lakes are also included within the ice distal and proglacial ice-contact counts. Two glaciers (East and West Twin glaciers) end in the same proglacial, moraine-dammed lake (Figure 7)

Type of lake	Count	Number of glaciers with this observation	Total summed area (km^2)	Minimum lake area (km^2)	Maximum lake area (km^2)	Count of moraine-dammed lakes
Proglacial (ice-contact) lake	47	41	58.4	0.006	12.62	3
Supraglacial lake	23	7	0.1	0.001	0.03	
Ice-dammed marginal lake	28	11	7.4	0.001	1.77	
Ice-distal lake	232		926.3	0.001	500.20	4
Tarn (ice-distal lake)	38		3.5	0.016	0.32	
Moraine dammed*	7	6	13.2	0.002	12.9	

TABLE 7 Glaciological features mapped around Juneau Icefield in 2019 from Sentinel imagery, with number of observations and elevation statistics where appropriate. Icefalls (points) is where a group of icefall-type crevasses have been mapped as a single icefall

Feature	Number of observations (area, km^2)	Mean elevation (m)	Range of elevation (m a.s.l.)	Standard deviation of elevation (m)	Number of glaciers with this observation
Icebergs	997				9
Primary stratification/foliation	599	1284	795–1776	224	
Deformed foliation	229	1290	345–1756	316	71
Longitudinal flowlines	348				32
Bergschrund	91	1798	1194–2240	202	22
Transverse crevasses	6075	1364	69–2313	465	199
Marginal crevasses	2603	882	103–2089	354	43
Icefall-type crevasses	4891	1481	810–2121	212	
Icefalls (points) (number of icefalls)	150				55
Ogives	926	939	237–1561	223	13
Longitudinal crevasses	1649	830	122–1937	400	40
Splaying crevasses	1043	421	25–1554	376	15
Rifts	6				1
Medial moraines	742				138
Disconnections (outlet glaciers)	77	1264	725–1876	256	14
Disconnections (valley glaciers)	99	1386	666–1996	276	52
Disconnections (mountain glaciers)	92	1393	652–2040	301	81
Disconnections (glacierets)	13	1371	1136–1724	207	17
Separations	59	1040	17–1698	402	26
Debris flows	10 (0.93 km^2)				10
Debris cover	110 (72.9 km^2)				111
Total	**20 809**				**949**

was much lower for outlet glaciers, with a mean of 2.4%. Glacierets in contrast had a mean of 33.9% debris cover. Glacierets that showed little sign of active flow in terms of crevassing or ductile deformation structures are apparently down-wasting, resulting in a darkening of the ice surface as the glacier ablates, advecting debris from within and accumulating both rocky and wind-blown debris and dust. On the whole, Juneau Icefield overwhelmingly constitutes clean-ice glaciers.

In addition to this surficial debris cover, debris flows or landslides emanating from the valley sides were observed on 10 glaciers. These debris flows are characterized by a thicker layer of debris with a rougher surface texture, a darker colour and a lobate form. Debris flows ranged in size from 0.01 to 0.27 km^2, with a total area of 0.92 km^2.

Medial moraines frequently dissect glaciers. They form in zones of lateral compression in the trunks of outlet and valley glaciers, especially where multiple accumulation basins are confluent. Mostly these are straight and aligned with the longitudinal foliation, but Gilkey Glacier exhibits some lateral folding of the longitudinal foliation and medial moraines (Figure 10).

Areas with stagnant ice (such as Norris Glacier Dead Branch; Figure 13) show few crevasses and little evidence of forward ice motion. These glaciers are typically debris covered, with folded medial moraines or longitudinal structures indicating deformation from inflowing ice. Debris-covered, stagnant ice is also apparent in marginal cirques alongside Taku Glacier. Here, tributaries have become disconnected from their feeder cirques, leading to cessation of ice flow into

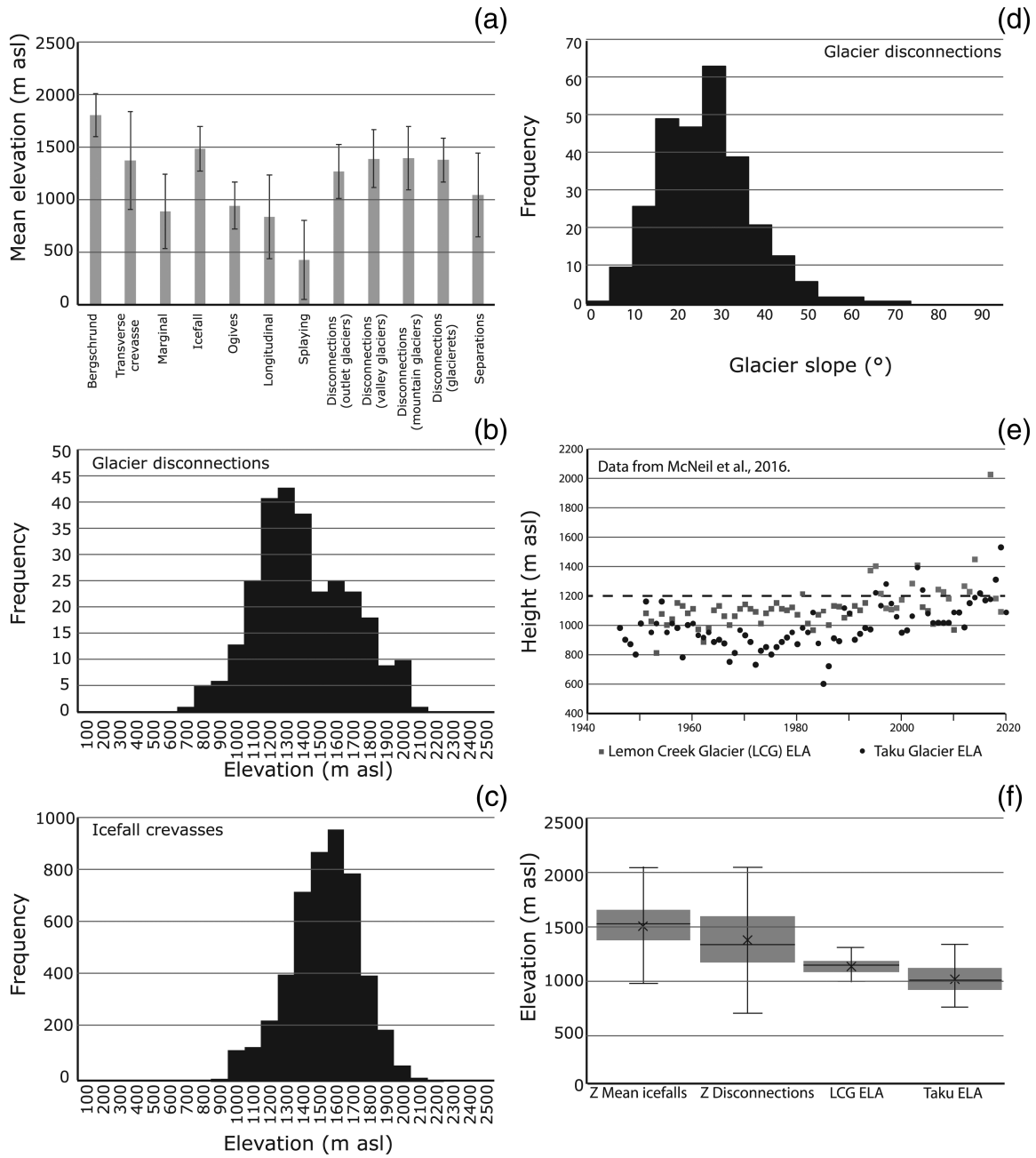


FIGURE 8 (a) Mean altitude of key structural features, with error bars showing one standard deviation (SD) around the mean. (b) Histogram of altitude of disconnections. (c) Histogram of altitude of icefall crevasses. (d) Histogram of slope of glacier disconnections. (e) Glacier equilibrium line altitude (ELA) data from Lemon Creek and Taku glaciers (data from McNeil et al., 2016, 2019). Black dashed line shows altitude of the plateau of Taku Glacier. (f) Box plots of the mean elevation of icefalls, the elevation of the disconnections and the ELAs of Taku and Lemon Creek glaciers.

the main trunk glacier. Medial moraines and longitudinal structures attest to the lack of inflow of ice from these side tributaries (Figure 13). Ice-flow changes of Taku Glacier during the 20th century have led to stagnation of glacier ice north of Goat Ridge. Around the periphery of Taku Glacier ablation zone, ice-marginal cirques are a prime candidate location for the formation of future ice-dammed lakes.

3.3.6 | Glacier separations and disconnections

Glacier separations ($n = 59$) and disconnections ($n = 281$) were mapped across the icefield and its peripheral glaciers (Figure 7). Disconnections were observed at 164 glaciers, with multiple disconnections occurring at numerous glaciers. Thirteen of the mapped disconnections were associated with glacierets, 92 with mountain glaciers, 77 with outlet glaciers and 99 with valley glaciers (Table 8). These disconnections occurred in places with a steep surface slope (mean 26.0°; Figure 8d). Disconnections occurred at a consistent height, with a mean altitude of 1354 m (SD 280) (Table 8; Figure 8a). The elevation of these is approximately normally distributed, with the peak of the distribution from 1200 to 1400 m a.s.l. (Figure 8b). The mean elevation of disconnections associated with glacierets is higher (1371 m) than outlet glaciers (1264 m), likely related to the higher Z_{med} for glacierets. The mean altitude of the disconnections is well below the mean Z_{med} of the glaciers (cf. Tables 4 and 8).

Glacier disconnections occur commonly in association with heavily crevassed terrain and icefalls, as a result of narrowing and thinning of ice over steep terrain. Elevation change data from

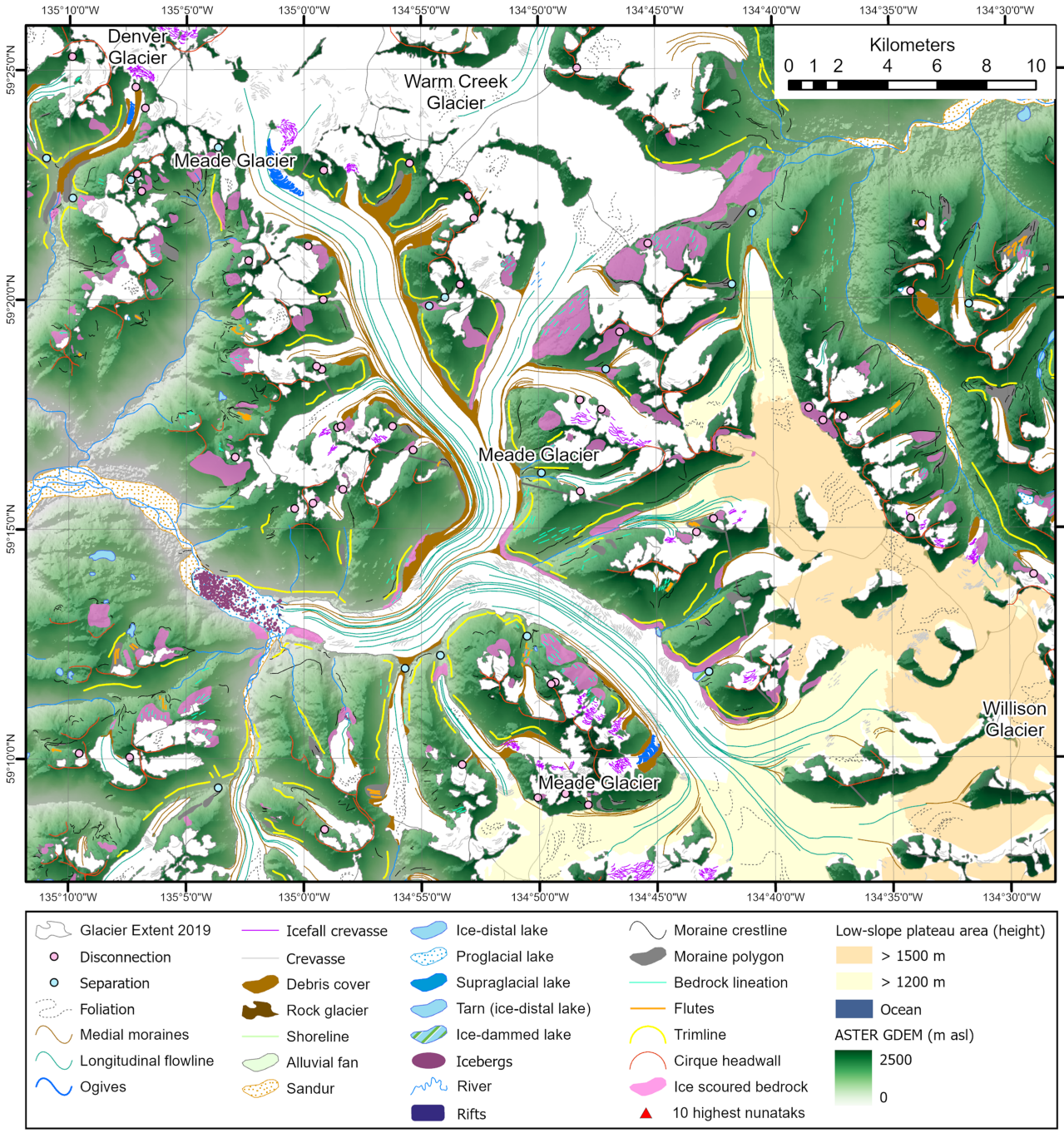


FIGURE 9 Glaciological and geomorphological map of Meade Glacier. Overlain on a hillshaded ASTER GDEM. [Color figure can be viewed at wileyonlinelibrary.com]

Hugonnet et al. (2021) shows that, while glacier thinning is concentrated on glacier tongues, it does now reach the elevation of the icefalls. There is thinning at, for example, Vaughan Lewis icefall on Gilkey Glacier (Figure 14b). This icefall thinned by an average of 0.9 m a^{-1} from 2000 to 2020 AD (data from Hugonnet et al., 2021). Gilkey Glacier is also associated with a number of tributary disconnections between the main trunk and the multiple accumulation basins in areas of steep ice-surface slope (Figure 10). Below the icefall, the lower ablation portions of the glacier tongue thinned by >4 m a^{-1} over the period from 2000 to 2020 AD (cf. Hugonnet et al., 2021). At Thiel Glacier, thinning over this time period in an area of steep ice-surface slope, icefalls and disconnections is 2.2 m a^{-1}.

Many disconnections between accumulation and ablation zones occur on valley glaciers with a clearly defined cirque headwall, where the ice-surface slope is steep and intensely crevassed. Eagle, Thiel and Denver glaciers are excellent examples (Figure 4). In contrast, although some of the largest outlet glaciers have icefalls within their main flow units, there is not yet sign of disconnection here, due to the thicker ice. Where outlet glaciers are thick enough to overwhelm subglacial topography (Ziemen et al., 2016) (e.g. Taku Glacier; Nolan et al., 1995, Norris Glacier main branch, Llewellyn Glacier, Meade Glacier south accumulation basin), there is no change in ice-surface slope and hence few icefalls observed forming at the edge of the plateau (Figure 6). However, there are disconnections associated with icefalls from smaller tributary basins to the outlet glacier trunks.

Glaciers associated with disconnections from their tributaries tended to have more debris cover than average (Table 9). Of the 164 glaciers associated with disconnections, 15 (9.1%) had >10% debris cover and

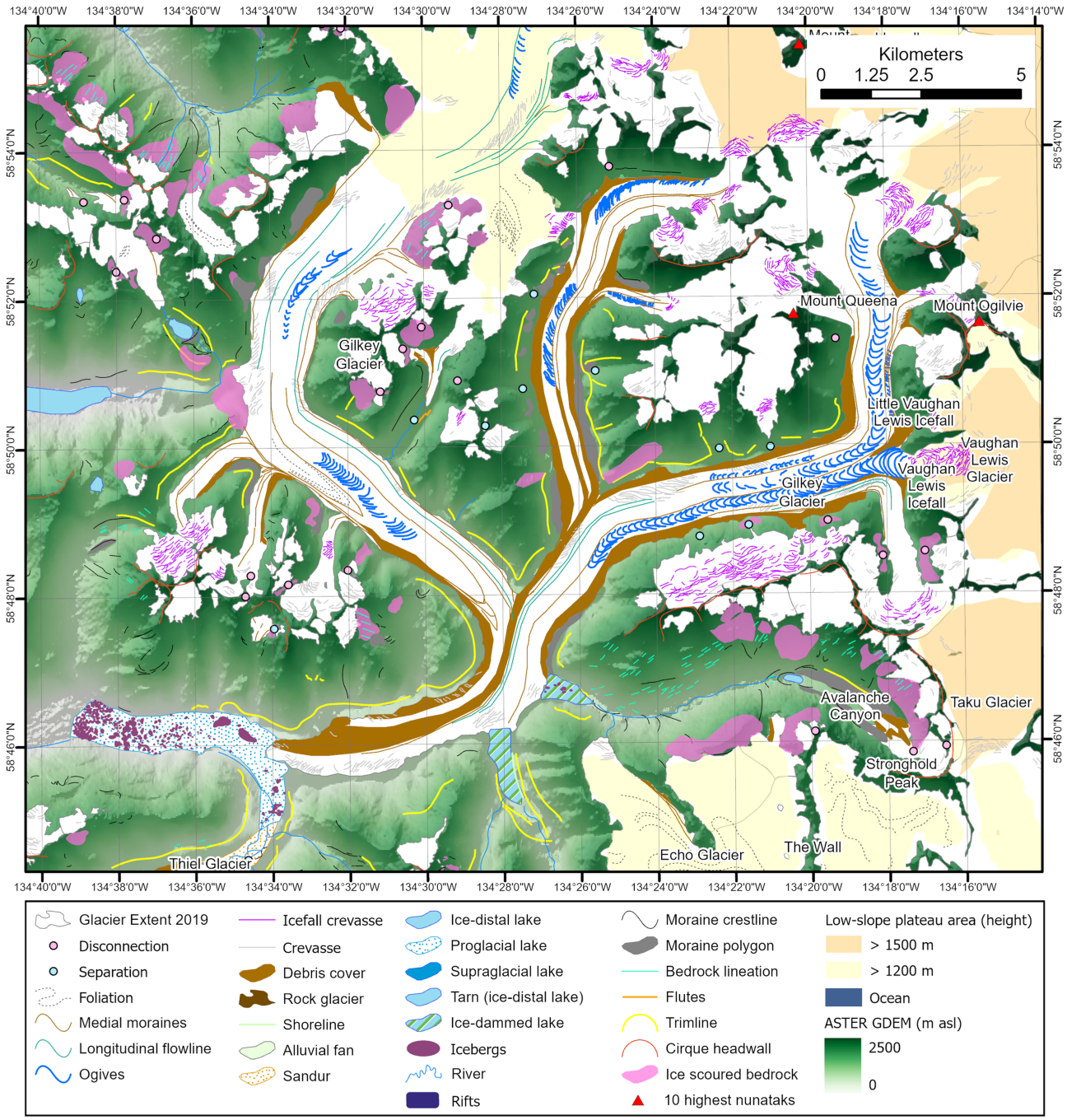


FIGURE 10 Geomorphological and glaciological map of Gilkey Glacier, Juneau Icefield. Overlain on a hillshaded ASTER GDEM. [Color figure can be viewed at wileyonlinelibrary.com]

50 (30.5%) had some debris cover. These values are higher than those for the 866 'normal' glaciers (i.e. those without disconnections) associated with neither disconnection nor tributary separation (Table 9). The mean percentage of debris-covered area was 2.63% for disconnected glaciers and 0.95% for other glaciers. A paired-sample Student's *t*-test assuming unequal variances showed that disconnected glaciers had more debris cover than 'normal' glaciers ($t = 2.63$, $p < 0.05$, d.f. = 211). Denver, Laughton and Thiel are examples of valley glaciers with particularly good examples of debris cover on the glacier tongue (Figure 4). For glaciers where at least one ice-flow unit is completely disconnected, there are clear signs of stagnation, including increased surficial debris and deformed longitudinal foliation (e.g. Thiel Glacier; Figure 4).

Tributary separations ($n = 59$) are clear in the valley floors where glaciers with multiple accumulation basins are undergoing recession. They typically occur on lower surface slopes than disconnections (Table 8). This will act to accelerate recession of the main trunk glacier, as it has lost an ice-flow tributary. These separations occur commonly for the larger outlet glaciers in the valley floors (Figure 7), developing as the icefield fragments.

4 | LANDFORM INVENTORY

Remote sensing mapping of Juneau Icefield has produced the first regional geomorphological map for the region (Figure 7). We identified over 10 200 geomorphological landforms (Table 10).

The Coast Mountains are drained by parabolic valleys. Close to the icefield, these are occupied by outlet glaciers; further from the

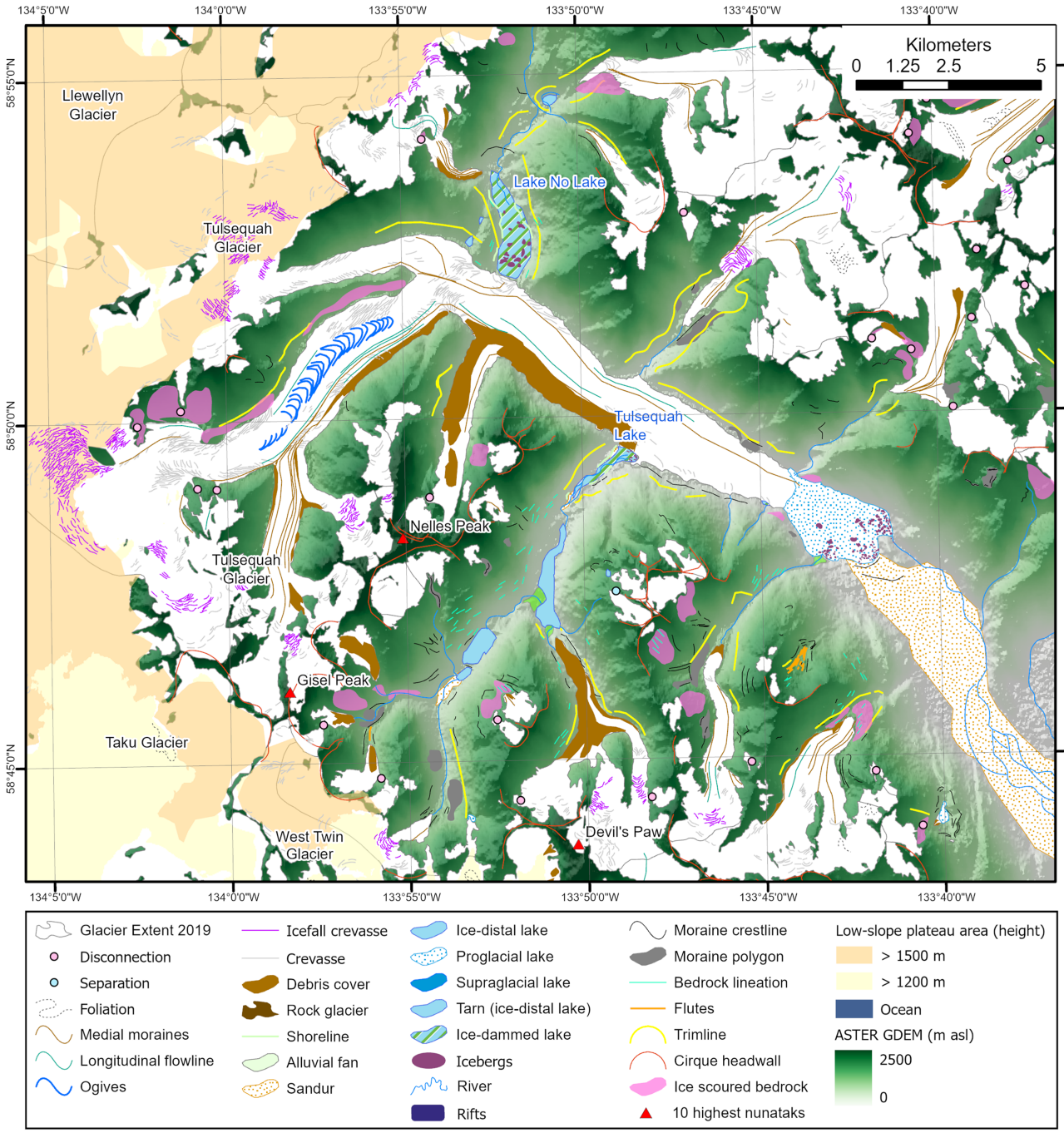


FIGURE 11 Geomorphological and glaciological map of Tulsequah Glacier, Juneau Icefield. Overlain on a hillshaded ASTER GDEM. [Color figure can be viewed at wileyonlinelibrary.com]

main icefield, they bear the hallmarks (e.g. roche moutonnée) of an enlarged icefield, likely formed during the Last Glacial Maximum under the Cordilleran Ice Sheet. The broader-scale geomorphology has the typical features of a glaciated landscape, including steep-sided arêtes, pyramidal peaks protruding through the icefield as nunataks, and cirques.

The forefields of numerous mountain glaciers largely comprise glacigenic sediment and ice-scoured bedrock; the latter typically on topographic highs inside the LIA terminal moraines. The plutonic geology of the region is susceptible to scouring and polish. In places the bedrock is characterized by smooth, polished bedrock and lineations (roche moutonnées) that trend down-valley towards the terminal moraines.

On glacier forefields within LIA terminal moraines, glacial sediment deposits are often characterized by elongate, parallel to sub-parallel lineations interpreted as flutes. Flutes are most apparent at the smaller mountain glaciers. These small-scale linear, elongated features are typically on the order of hundreds of metres long and tens of metres wide. Some features continue downstream from roche moutonnées and other topographic highs. In places, distinguishing between fluted glacial sediments and roche moutonnées on bedrock is challenging, particularly as they often occur adjacent to each other. However, for each glacier, the orientation of these linear structures is consistent. The areas in front of some glaciers (e.g. Eagle, Herbert, Mendenhall) also contain some forested land, which impedes mapping.

In some places, larger ridges continue the pattern of medial moraines and debris cover observed on the ice surface. These are interpreted as the continuation of medial moraines from the ice

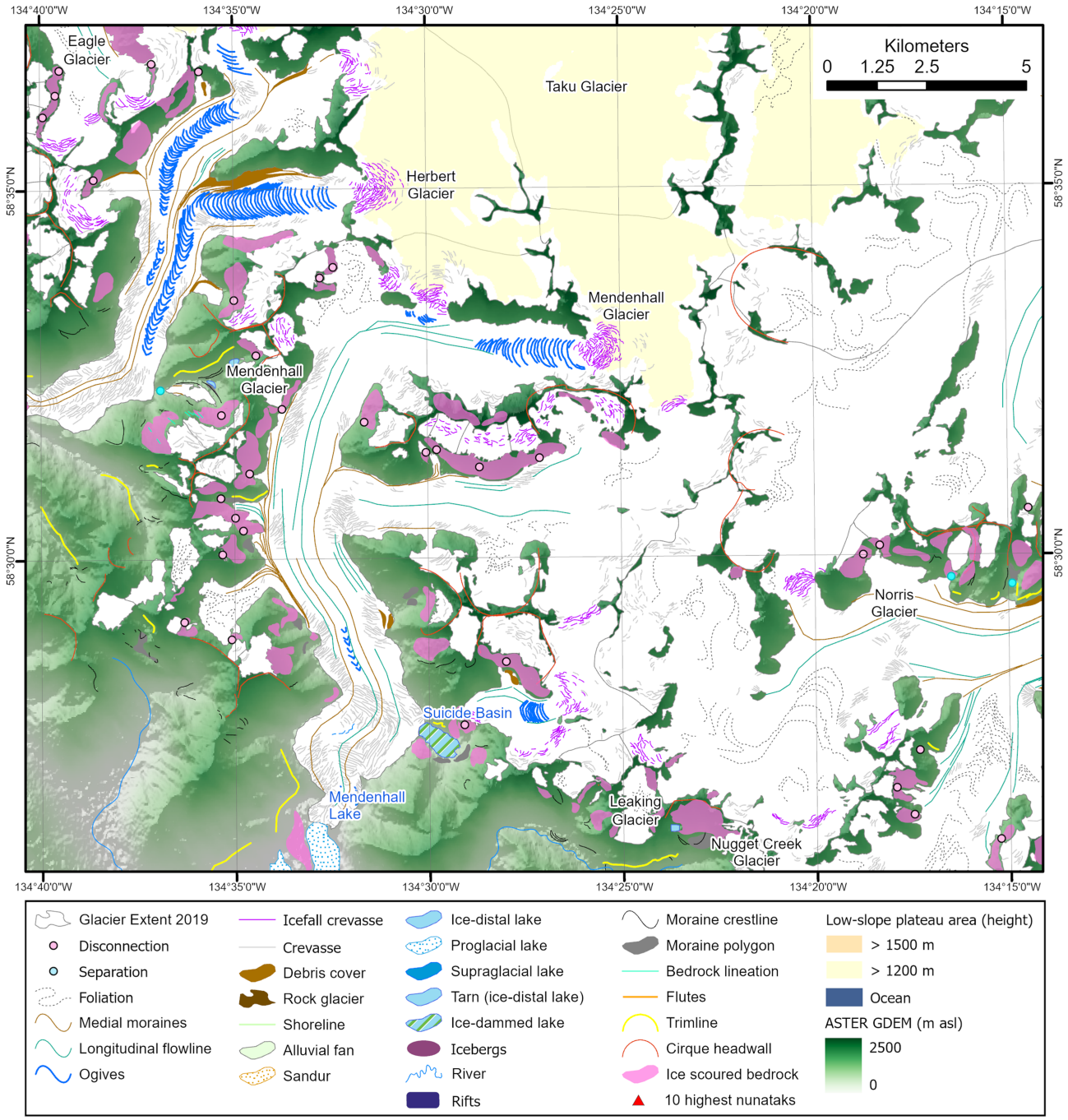


FIGURE 12 Glaciological and geomorphological map of Mendenhall Glacier, Juneau Icefield. Overlain on a hillshaded ASTER GDEM. The terminus of Mendenhall Glacier and Mendenhall Lake is shown in Figure 14e. [Color figure can be viewed at wileyonlinelibrary.com]

surface, rather than as a result of subglacial processes, and are mapped as moraines.

Trimlines are pervasive around the termini of valley glaciers and outlet glaciers (cf. Heusser, 2007). They sometimes connect down-valley with lateral and terminal moraines and reflect ice thickness during the neoglaciation (Rootes & Clark, 2020). They are characterized by sub-horizontal lines on valley sides, with non-vegetated land below and vegetated land above.

Moraine complexes are typically multi-crested, with densely spaced nested terminal moraine crests for most glaciers. There are generally few recessional moraines inside the main moraine complexes (e.g. Llewellyn and adjacent glaciers; Figure 16 and most mountain glaciers; Figures 7 and 9). Previous field surveys describe the sediments as weakly stratified diamictons, with abundant striated and faceted clasts (Clague et al., 2010). This is typical of polythermal or warm-based ice (Benn & Lukas, 2006). The advance of Taku Glacier throughout the late 20th century, for example, led to the formation of push moraines, locally uplifting proglacial sediments (Kuriger et al., 2006). These form ridges up to 6 m high, composed of boulders and cobbles in a diamicton.

Most glaciers have one main moraine complex, with an area largely devoid of moraines between the main complex and the current glacier tongue, indicating largely continuous recession since the LIA neoglacial maximum. This area is characterized by flutes and bedrock lineations. In some places, the pattern of moraines indicates previous separations of glacier trunk and tributaries as recession proceeded.

Sandur are well developed in front of the larger land-terminating outlet glaciers. Sandur comprise braided sediment-rich streams with a

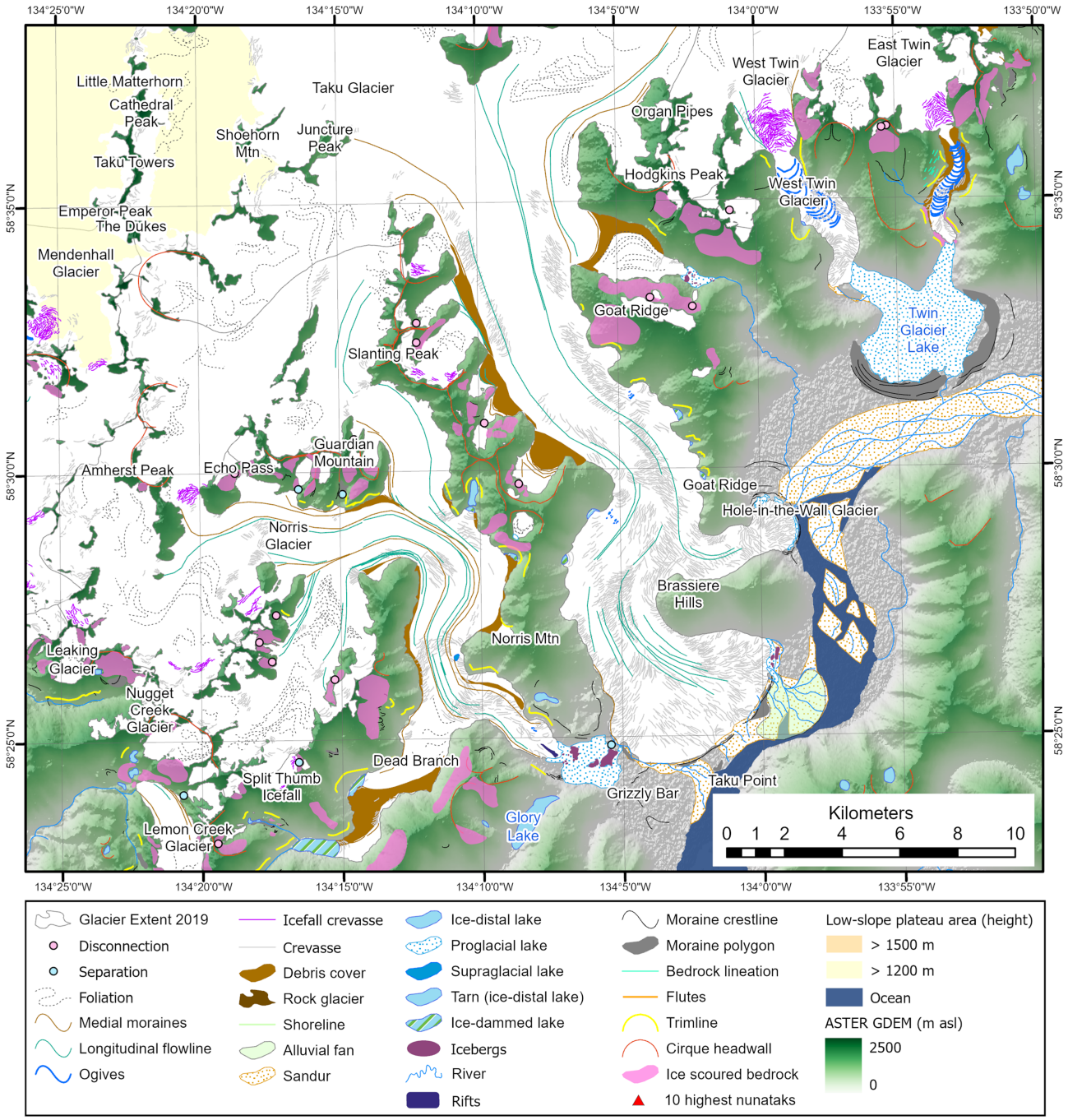


FIGURE 13 Glaciology and glacial geomorphology for Norris, Taku and East and West Twin glaciers. Overlain on a hillshaded ASTER GDEM. [Color figure can be viewed at wileyonlinelibrary.com]

low gradient. They are particularly well developed draining the proglacial lakes in front of Tulsequah (Figure 11), West and East Twin and Taku (Figure 13), Meade (Figure 9), Field, Llewellyn and Warm Creek glaciers. Smaller sandur are found draining some valley glaciers, including Thiel Glacier.

5 | DISCUSSION

5.1 | Ice flow and thermal regime

The spatial distribution and characteristics of brittle deformation in the form of crevasses on the glaciers of Juneau Icefield are similar to those observed in many other glaciers, with crevasses opening in the direction of maximum tension (Colgan et al., 2016; Jiskoot et al., 2017; Nye, 1952). Flow units within the trunks of the valley glaciers and outlet glaciers remain independent and reflect their individual accumulation areas. Glaciers are characterized by arcuate upward and transverse crevasses in regions of longitudinal extending flow. They frequently occur upstream of icefalls (e.g. Figures 10 and 11; Gilkey and Tulsequah glaciers). Longitudinal crevasses and splaying crevasses occur in regions of lateral extension in the middle parts of the glacier trunk; for example, at locations of valley widening and points where the trunk glacier has an abrupt turn. In these outlet glaciers, which are unconfined in their accumulation areas and strongly confined in their trunks, drag with the valley wall causes marginal or chevron crevasses with angles oriented up-glacier at 45° or more in regions with a uniform velocity (cf. Jiskoot et al., 2017). This



FIGURE 14 (a) Icefall and ogives on Gilkey Glacier, taken by Austin Post mid-20th century (Wikimedia commons). *Note*: the ogives becoming increasingly deformed down-ice of the icefall. (b) Vaughan Lewis (right) and Little Vaughan Lewis icefalls (left) on Gilkey Glacier, taken in 1955 by Austin Post (Wikimedia commons). These are the same icefalls as observed in panel A. Little Vaughan Lewis icefall is now disconnected from Gilkey Glacier. (c) Photograph looking down-glacier from above the icefall on Gilkey Glacier, taken by Ron Clausen (Wikimedia commons). (d) The plateau accumulation area (1100 m a.s.l.) of Taku Glacier, with the Taku Towers nunatak. (e) Terminus of Mendenhall Glacier in 2014. Credit: Robert McNabb. (f) Terminus of Norris and Taku glaciers in 1975, showing the build-up of Grizzly Bar moraine, taken by Mauri Pelto. [Color figure can be viewed at wileyonlinelibrary.com]

emphasizes the dominance of simple shear in the trunks of these outlet glaciers. Towards the terminus, longitudinal and splaying crevasses become more common, as valley glaciers experience slower, compressive flow at their snout, and lateral extension on the wider valley floor (Hambrey & Lawson, 2000).

Evidence of ductile deformation includes a typical progression of primary stratification, deformed into folded primary stratification and then longitudinal foliation. This progression illustrates the dominance of pure and simple shear in these glaciers, which acts to attenuate the folds of limbs and eventually transpose the primary stratification (Hambrey & Lawson, 2000; Jennings et al., 2014). Longitudinal flowlines are predominant in valley glaciers and outlet glaciers with broad accumulation areas and multiple basins, feeding tributaries that meet in one valley glacier trunk. This results in increased lateral compression, with narrowing of the flow unit, and favours the development of longitudinal foliation. This lateral compression also favours

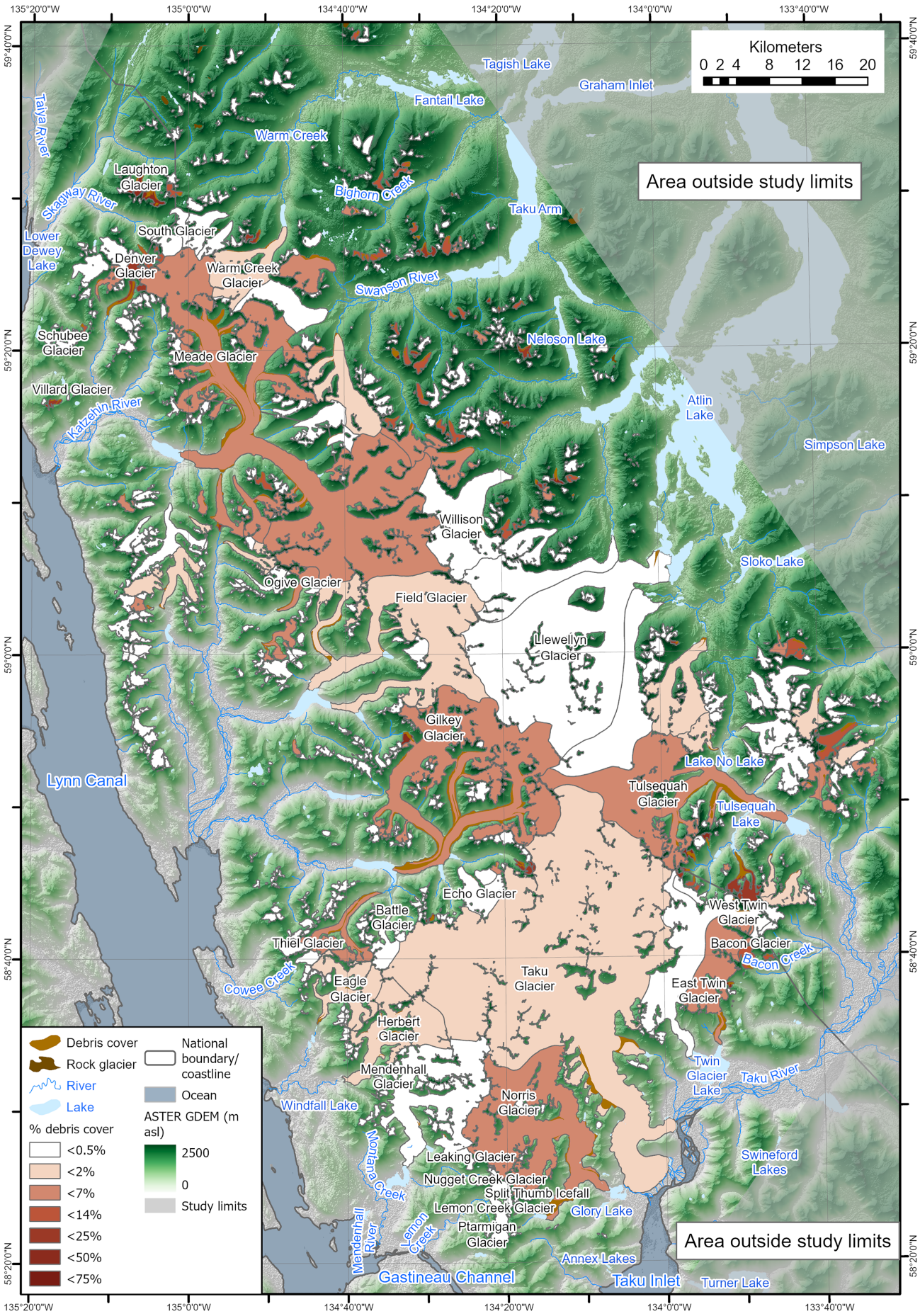


FIGURE 15 Percentage of debris cover for glaciers of and around Juneau Icefield. Overlain on hillshaded ASTER GDEM. [Color figure can be viewed at wileyonlinelibrary.com]

TABLE 8 Descriptive statistics for disconnections and separations across the study area

Glacier type	Count	Mean altitude (m a.s.l.)	Standard deviation	Mean slope (°)	Standard deviation	Minimum altitude (m a.s.l.)	Maximum altitude (m a.s.l.)
Mountain glacier	92	1392.6	301.3	26.6	10.0	785.0	2040.0
Valley glacier	99	1385.5	276.2	25.0	11.2	666.3	1996.0
Outlet glacier	77	1264.3	256.2	26.7	9.3	725.1	1876.1
Glacieret	13	1371.1	207.1	24.4	10.9	1136.4	1724.0
All disconnections	**281**	**1354.0**	**280.9**	**26.0**	**10.3**	**666.3**	**2040.0**
Separations	59	1039.7	401.6	15.1	10.9	17.0	1745.0

TABLE 9 Percentage of 'disconnected' and 'normal' glaciers with debris cover

	Count	Mean % debris cover	Percentage with >10% debris cover	Percentage with any debris cover
'Disconnected' glaciers	164	2.63	8.80%	26.90%
'Normal' glaciers	860	0.95	2.90%	6.30%

TABLE 10 Landform inventory for Juneau Icefield

Features	Number of observations	Total area (km^2)	Mean area (km^2)
Glaciers	1050	3816.4	3.6
Moraine ridge crests	3602		
Polygons of glacial sediment/moraine	351	49.2	0.15
Flutes	649		
Bedrock lineation (roche moutonnée)	1671		
Trimlines	537		
Sandur	41	140.8	3.5
Cirque headwall	823		
Shorelines	22		
Polygons of ice-scoured bedrock	737	220.3	0.3
Alluvial fan	19	4.9	0.26
Rivers	362		
Proglacial, ice-contact lakes	47	58.4	
Ice-dammed lake	28	7.8	
Non-ice-contact lake	232	926.3	
Tarn in cirque	38	3.5	
Rock glacier	10	3.2	0.32
Total	**10 219**	**5230.8**	

longitudinal extension to ensure conservation of mass (cf. Jennings et al., 2014), which increases the rate of formation of longitudinal foliation. Ogives are further evidence of ductile deformation and simple shear, and are characteristic of active-temperate glaciers with icefalls (Jennings & Hambrey, 2021). The number of supraglacial streams and lakes, and the glacier lake area, is very small, suggesting that most meltwater in the ablation area makes its way rapidly to the glacier bed and drains subglacially, which also suggests temperate ice.

The association of longitudinal flowlines, deformed foliation and these crevasses suggests a temperate thermal regime, with ice flow by both internal deformation of the ice and basal sliding. Together, these structures are common in temperate valley glaciers where there is strong lateral compressive flow (Goodsell, Hambrey, & Glasser, 2005; Jennings et al., 2014; Jiskoot et al., 2017). The dense crevasses attest to dynamic flow, with longitudinal extension in the along-flow direction as the glaciers descend down the valley or slope. The smaller valley glaciers and glacierets typically have lower velocities and fewer crevasses, although transverse crevasses are apparent on some steep mountain glaciers. There is only evidence for former surge activity on Gilkey Glacier, with looped medial moraines and longitudinal flow structures (Figure 10) (Copland et al., 2003; Evans & Rea, 2003; Grant et al., 2009). This is the first documented evidence of former surging on Juneau Icefield.

Although many glaciers show evidence of active-temperate ice, there is also increasing stagnation evident for some glaciers, such as Thiel, Eagle and Denver glaciers (Figure 4). Typically, evidence of

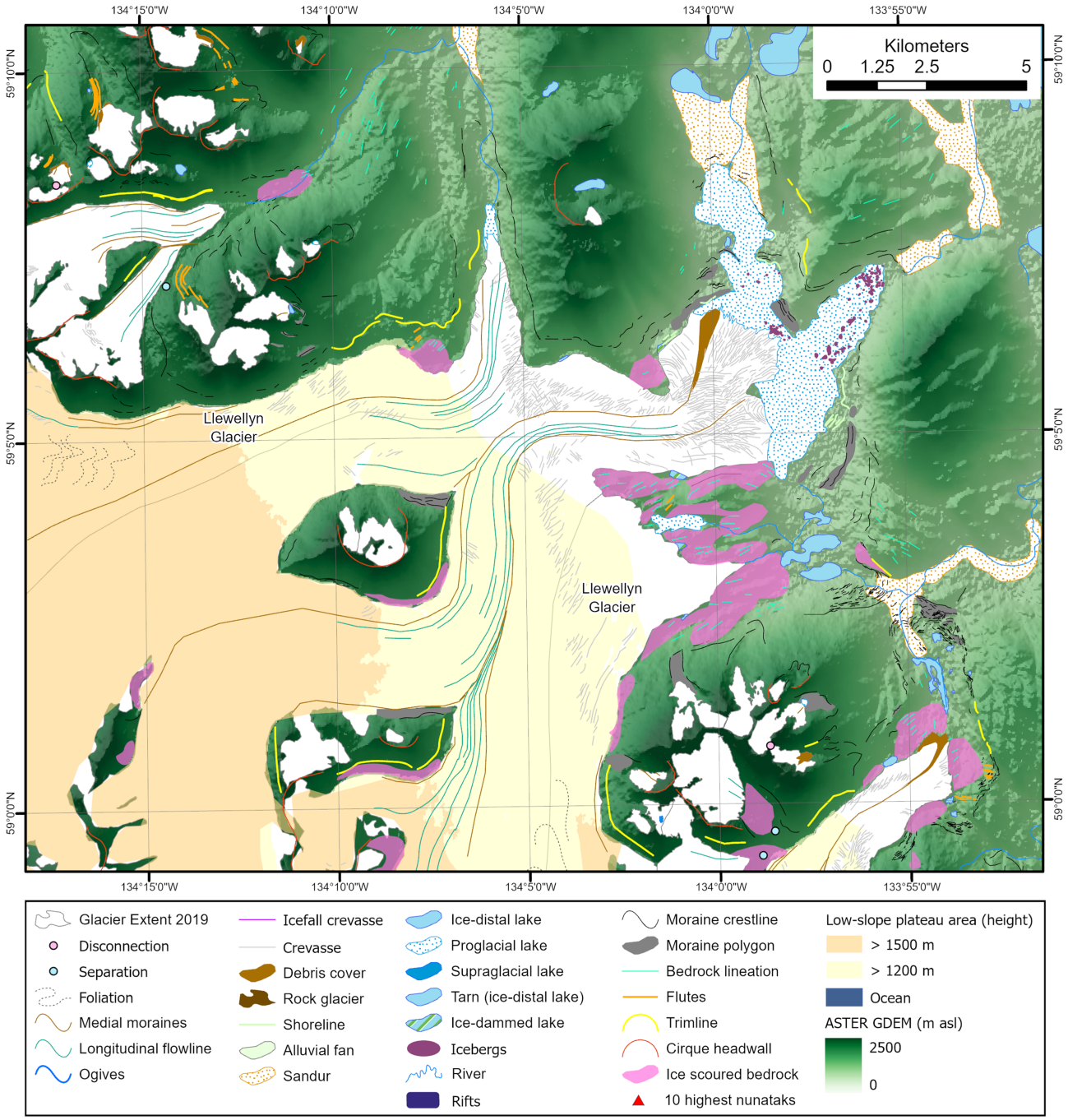


FIGURE 16 Glaciological and geomorphological map of Llewellyn Glacier and adjacent glaciers. Overlain on a hillshaded ASTER GDEM. [Color figure can be viewed at wileyonlinelibrary.com]

stagnation was found at glaciers that have undergone significant separation and disconnection, with disconnected trunks being prone to collecting debris cover.

5.2 | Glacial lakes

Ice-dammed lakes, formed in lateral valleys of outlet glacier trunks as they become ice free, and between the glacier and the valley walls (Geertsema & Clague, 2005; Marcus, 1960; Stone, 1963), represent a hazard at some glaciers (Kienholz et al., 2020). Ice-dammed lakes were observed for Taku, Norris, Field, Tulsequah, Mendenhall and Gilkey glaciers. These lakes usually drain subglacially during each summer melt season (Marcus, 1960), emptying over 4–5 days in an outburst flood (Geertsema & Clague, 2005). Suicide Basin, dammed by Mendenhall Glacier (Figure 12), has released annual glacier lake outburst floods since 2011 (Kienholz et al., 2020). Although it has an area of only 0.7 km^2, in the 2018 and 2019 outburst flood events, Suicide Basin released ~30 × 10^6 m^3 of water over the course of 4–5 days (Kienholz et al., 2020).

This new inventory shows 28 lakes dammed by 11 glaciers, nearly three times the 10 ice-dammed lakes previously mapped (Stone, 1963). An increase in the number and volume of water stored in ice-dammed lakes as the icefield continues to recede and fragment may increase the hazard posted by ice-dammed lakes over the coming century. However, a thorough hazard assessment was not carried out as part of this study, and these lakes are not necessarily dangerous.

Proglacial lakes were mapped in front of 47 glaciers, including large lakes in front of 12 icefield outlet glaciers. As the low-gradient

outlet glaciers in the relatively flat valley bottoms thin and increasingly reach flotation in proglacial lakes, this may exacerbate calving, terminus thinning and stretching, and increase frontal ablation. Buoyancy-driven calving and accelerated retreat has previously been observed at Mendenhall Glacier (Boyce et al., 2007; Motyka et al., 2002). However, no icebergs were mapped here in this study (Figure 12), suggesting a change in frontal dynamics since 2004 as it receded into shallower water. Indeed, some of the terminus is now on land. Instead, other glaciers where voluminous calving is noted (e.g. Tulsequah, Gilkey, Meade, Field) may now be prone to this process. Particularly large and tabular icebergs were noted in front of Field Glacier, suggesting partial flotation and that calving is an important component of mass loss here. The new moats in front of Taku Glacier are likely to grow as the ice thins and recedes into the substantial (~600 m) over-deepening upstream from the terminus (Nolan et al., 1995), and is likely to eventually re-initiate calving (McNeil et al., 2021). In other places with more gradient, such as East Twin Glacier, the glaciers may recede out of their proglacial lakes, ceasing calving, in a similar way to Mendenhall Glacier. Ultimately, given that of the 40 glaciers that terminate in proglacial lakes, icebergs are observed in front of only eight outlet glaciers, calving and frontal ablation is likely to be but a small component of all mass loss from glaciers in this region.

5.3 | Topographic controls on glacier recession

Juneau Icefield is receding rapidly, with the loss of 63 glaciers and 422.3 km^2 (10.0%) of ice from 2005 to 2019 AD. This recession is in line with previous work on volumetric change (Berthier et al., 2018; Hugonnet et al., 2021; Jakob et al., 2021). Differencing of DEMs from 2000 to 2019 over the icefield (data available from Hugonnet et al., 2021) shows particularly rapid down-wasting on the lower tongues of large outlet and valley glaciers, including Tulsequah, Gilkey, Thiel, Eagle, Meade, Warm Creek, Ogive, East Twin, Battle and Field glaciers, whilst the thicker, larger glaciers such as Willison, Norris, Taku, Llewellyn and Mendenhall show lower rates of ice-surface lowering. Warming trends in the region (Thoman & Walsh, 2019) have therefore caused rising ELAs (McNeil et al., 2020) and thinning of glaciers across the Juneau region (Hugonnet et al., 2021).

Glacier disconnections found at peripheral glaciers around the icefield have strong implications for the future mass wastage of the continuous portion of the icefield. These fragmentation processes result in decreased down-glacier nourishment from higher elevations (Rippin et al., 2020). Stagnation and down-wasting of isolated glacier tongues below zones of fragmentation (e.g. Thiel and Eagle glaciers) is clear from the structural mapping, increased debris cover and DEM differencing data available from Hugonnet et al. (2021). Indeed, the glaciers with particularly severe surface lowering are all undergoing extensive disconnections in key flow units. While both separations and disconnections directly impact glacier recession, we specifically highlight the implications to future Juneau Icefield recession resulting from icefall disconnections.

Thirteen of the 40 outlet glaciers that draw ice directly from the plateau of Juneau Icefield (including Gilkey, Meade, Ogive, Mendenhall, Herbert, Bacon, Battle, East and West Twin, Tulsequah and Field glaciers) have ablation zones currently joined to the plateau via icefalls. Future disconnections occurring in these outlet glaciers may accelerate the recession of the ablation portions of 1325.7 km^2 of the main Juneau Icefield. Additionally, there are 11 valley glaciers immediately contiguous with the icefield (including Thiel, Denver, Eagle and South glaciers) with narrowing icefalls in this zone, with an additional area of 132.9 km^2. Increased ablation of glacier tongues, especially on thinner glaciers with icefalls, is therefore likely to increase, driving further icefield fragmentation. Indeed, a narrowing of the icefall at East Twin Glacier is already evident (Figure 13), with rapid thinning below the icefall (data from Hugonnet et al., 2021).

These disconnections are topographically controlled, occurring on steep slopes at a consistent altitude (mean 1354 m a.s.l., SD 281). Glacier ELAs (mean 1172 m, SD 150 m, for Taku Glacier; Figure 8e) now increasingly intersect the mean elevation of icefalls around the icefield plateau (Table 7 and Figure 8f; icefall crevasses have a mean altitude of 1481 m a.s.l., SD 212). As icefalls are increasingly within the ablation zone, thinning and eventual disconnection of these flow units is likely.

As outlet glaciers thin, underlying bedrock topography becomes more important in controlling ice flow; thus, thinning glaciers may experience an increase in the number of heavily crevassed areas. Increased crevassing increases surface roughness and increases latent and sensible heat fluxes at the ice surface, resulting in increased energy gain at the ice surface (Colgan et al., 2016). The appearance of bare rock within the glacier boundaries will increase melt due to the albedo-melt feedback. Longwave radiation received from the surrounding dark rock can increase nearby ice melt (Hock & Holmgren, 2005; Jiskoot et al., 2009). Continued rapid thinning and the appearance of more bare rock within the icefield is therefore increasingly likely.

The hypsometry of top-heavy icefields such as Juneau, where icefalls are common in areas of steep ice-surface slope around a plateau, means that they may be more susceptible to these processes. Although disconnections are yet to be systematically mapped for other icefields, they have been observed for Columbia Icefield (Rippin et al., 2020), especially in areas of icefalls. Glacier disconnections have also been observed for some plateau icefields in Norway, such as Svartisen (Boston & Lukas, 2019) and Jostedalsbreen (Laute & Beylich, 2021). Alaska has some of the world's largest plateau icefields, including Harding Icefield and Stikine Ice Cap, both of which have hypsometric breaks like Juneau Icefield. Glaciological assessments are needed for these regions to determine whether disconnections are occurring in areas of steep ice-surface slope in these regions as well.

Alongside this process, ongoing recession of these glaciers has resulted in separation of glacier tongues in the valleys. This effectively has a similar effect to glacier disconnection, as it will act to accelerate ongoing glacier recession by reducing the accumulation area for the main glacier tongue. The recession of tributary glaciers will therefore contribute to fragmentation and an acceleration of glacier recession across the icefield.

A final topographic control that is driving the rapid recession observed on this icefield is that the glacier ELAs (e.g. Lemon Creek and Taku glaciers; McNeil et al., 2020) are now reaching the plateau area (above 1200–1500 m a.s.l.; Figure 8e). As glacier ELAs reach above this area, the low surface slope of the plateau means that further small rises in the ELA will drive increasingly large losses of accumulation area in these top-heavy outlet glaciers, resulting in a declining surface mass balance. The low-slope accumulation area is usually very thick ice (Millan et al., 2022), so there is potential here for an altitude mass-balance feedback (cf. Huss et al., 2012; Sass

et al., 2017) as the regional ELA approaches the lower surface slopes of the plateau area. This process will drive further rapid recession and fragmentation of the icefield, since the icefield cannot readjust readily by receding up-valley in the same way as a mountain glacier (cf. Zekollari et al., 2017).

5.4 | Debris cover and albedo

Juneau Icefield is largely comprised of clean-ice glaciers; 95.7% of glaciers have <10% debris cover. The total debris-covered area is only 0.02% of the entire glacier area of the Juneau Icefield region. This is in contrast to other parts of Alaska, where the total rock debris-covered glacier area is 38.6% (Herreid & Pellicciotti, 2020), and the Northern Patagonian Icefield, with 7.9% debris cover in 2015 (Glasser et al., 2016). The debris cover over the glaciers of Juneau Icefield is thin, and it does not exhibit the typical features found in debris-covered glacier tongues, in Alaska and other places, such as ice cliffs and supraglacial ponds (Anderson et al., 2021).

This paucity of debris is likely due the durable, granitic lithologies of the bedrock, which limit rockfall potential, and also because the plateau setting limits the amount of bedrock areas above the ice in the accumulation zone. This contrasts with regions where more friable, sedimentary and volcanic lithologies dominate (e.g. Davies et al., 2013). Some small mountain glaciers and glacierets are down-wasting and stagnating, and these glaciers are accumulating more coarse debris cover from supraglacial rockfalls.

The debris cover across Juneau Icefield is superficial, and amounts to a darkening of the glacier surface, likely generating variance in the regional mass balance. Deposition of superficial black debris across glacier tongues, especially when ice velocities slow as a result of up-glacier disconnections, is sufficient to change the glacier surface albedo, leading to increased glacier melting (Nagorski et al., 2019).

5.5 | Glacial landsystems

The Juneau Icefield landsystem is characterized by the upland plateau, surrounded by deep glacial valleys. The large plateau sustains extensive glaciers that reach low altitudes, with the largest glacier (Taku) reaching sea level. Most of the glacier tongues draining from the plateau terminate in laterally constrained valleys, but piedmont lobes with laterally spreading ice form at the terminus of the largest glaciers, that extend beyond the confines of the valley walls onto lowland flat areas. Multiple outlet glaciers are characterized by icefalls on their trunks as they drain down from the plateau, except for the largest and thickest glaciers (e.g. Taku, Norris), whose ice-surface slopes are largely unaltered by bed topography. Many of the larger outlet glaciers terminate in proglacial lakes. As they thin, this may encourage terminus flotation, increased calving and further recession (cf. Boyce et al., 2007), until the glaciers eventually recede to the shallower, ice-proximal parts of the over-deepening.

Outlet and valley glaciers are surrounded by moraines, with ice-moulded bedrock and roche moutonnées visible within the valleys and in recently deglacierized regions. These moraines are largely a main moraine complex, enclosing an area with sparse moraines (e.g. Llewellyn Glacier; Figure 16), as opposed to continuous sequences of recessional moraines as seen in Scotland relating to the Loch Lomond Stadial (Bickerdike et al., 2018; Boston & Lukas, 2019). Gilkey, Field, Llewellyn and Meade have particularly few recessional moraines visible, as they retreat into lake basins. This suggests that after recession began, the glaciers remained in disequilibrium with continuous retreat, with recession being interrupted by only a few stillstands or readvances. Less prominent stillstands may have been removed by fluvial activity. The presence of flutes behind the moraine complex is indicative of continuous recession without advances, characterized by glaciers with continued forward momentum even during recession.

Moraines that pre-date the latest Holocene readvance, during the LIA, are not prevalent in the study area. Holocene neoglacials prior to the LIA in this area were typically restricted in extent, and smaller than the LIA. The lack of older moraines may indicate that landforms deposited during the Younger Dryas and Last Glacial Maximum were not formed in this area. Numerical modelling does suggest a larger Cordilleran Ice Sheet in this area at 12 ka (Seguinot et al., 2016). Further work is required to establish whether this was the case, and the potential mechanisms behind it.

The landform assemblage found in the valleys is characteristic of those deposited by warm-based glaciers, with evidence for glacial transport and deposition. Lateral meltwater channels, which are often associated with cold-based ice on the plateau and at higher elevations, are characteristic of some plateau icefields (Bickerdike et al., 2018; Boston & Lukas, 2019), but were not observed in the satellite imagery over Juneau Icefield. Rather, ice-scoured bedrock was observed at high elevations across the icefield, suggesting active glacier erosion even on parts of the plateau. The paucity of supraglacial meltwater and the regular drainage of contemporary ice-dammed ice-marginal lakes today also points to an active subglacial hydrological system in the outlet and valley glaciers, with surficial meltwater rapidly finding its way to the base of the glacier and draining. This assemblage of landforms and contemporary structures suggests that both the present-day and the LIA neoglaciation in this area was characterized by temperate glaciation. Analysis of the landforms and the structural glaciology in tandem provides an unusually clear insight into the glacial thermal regime, ice dynamics, processes of landform generation and implications for contemporary glacier dynamics.

The landsystem associated with glaciers that have undergone significant disconnection is likely to be rather different. Here, once glaciers have passed a key glaciological threshold, glacier tongues stagnate, with decreased forward momentum and increased debris cover. The thinner glaciers flow more slowly due to decreased gravitational driving stress (Bradwell et al., 2013; Cuffey & Paterson, 2010). The down-wasting of these glacier tongues leads to an alternative landsystem development, dominated by ice-cored moraine, rather than moraine and flute formation (cf. Bradwell et al., 2013). This is already evident in front of Eagle and Thiel glaciers, for example. As glacier recession proceeds, the dynamic glaciological switch in these glaciers will be increasingly visible in the landform record.

CONCLUSIONS

We provide detailed icefield-wide glaciological, structural and geomorphological mapping for a plateau icefield in Alaska, and consider the implications of these structures for ice flow and glacier mass balance. We have mapped 31 028 landforms, including 1050 glaciers and

20 809 glacier structures for one of the largest plateau icefields in the world. Juneau Icefield and its peripheral glaciers covered $3816.4 \pm 15.9\ km^2$ in 2019, shrinking from $4238.4 \pm 47.6\ km^2$ in 2005, equating to an area loss of 10.0%, or $30.2\ km^2\ a^{-1}$. In total, 63 glaciers disappeared between 2005 and 2019 AD. We mapped 47 proglacial ice-contact lakes covering $58.4\ km^2$, and 28 marginal ice-dammed lakes that drain underneath the ice each summer. These lakes are forming in areas where tributary glaciers are receding or the valley tongue is shrinking laterally from the valley side, and this process is likely to continue as the icefield continues to recede and tributary separations continue. We also mapped seven moraine-dammed lakes, covering a total area of $13.2\ km^2$. Icebergs were mapped in nine proglacial lakes, with substantial calving activity mapped in front of Gilkey, Meade, Field, Llewellyn and Tulsequah glaciers.

Structures mapped on the ice surface include crevasses and icefalls, ogives, longitudinal foliation, medial moraines, debris cover, supraglacial meltwater and locations of glacier disconnections and separations. Finally, we performed an integrated assessment of neoglacial moraines, glacial lakes, trimlines, flutes and cirques.

Debris cover on the icefield is thin and superficial, and mainly comprises dust and black carbon accumulating on the ice surface. This is occurring especially where glaciers have undergone significant disconnection in key ice-flow units, and where ice flow is subsequently reduced. This process is likely to increase ablation if debris continues to accrete on the ice surface, altering the icefield's overwhelming dominance of clean-ice glaciers.

Together, these structures and landforms are indicative of a temperate landsystem, with active-temperate outlet glaciers draining the plateau accumulation area, both today (2019 AD) and during the LIA, the most recent neoglaciation. The LIA glacier landform record indicates a landsystem and glacier motion similar to that indicated by modern structural mapping. There is evidence of some stillstands and small readvances within the LIA moraine limits, indicating some periods of 20th-century glacier stabilization.

This mapping provides new insights into the interactions between topography and glaciology, and how new processes such as glacier disconnections and separations may influence the Juneau Icefield in coming years. Specifically, as ELAs increasingly intersect the elevation range of the numerous large icefalls draining the plateau of the icefield, disconnections will also increase. This process acts to decrease nourishment of the glacier tongue and encourage downwasting. Combined with rising snowlines, which act to rapidly reduce the available accumulation area on the plateau, this new process could accelerate recession for Juneau Icefield and other plateau icefields worldwide. We argue that glaciers with hypsometric steps and steep icefalls that intersect with the elevation of the regional ELA may be particularly predisposed to glacier disconnections between accumulation and ablation areas, and that this may act to reduce downstream ice flow and hasten glacier recession. Glacier structural analysis is therefore key to understanding non-linear controls on plateau icefield behaviour. These processes will accelerate outlet glacier recession and icefield fragmentation as even if ablation rates remain constant, the threshold glaciological behaviour observed will accelerate the link between ablation and glacier recession. The full dataset is available in the online Supplementary Information as ESRI Shapefiles and an A0 map.

ACKNOWLEDGEMENTS

JE acknowledges support from a NERC independent fellowship award (NE/R014574/1). We thank Jen Thornton, cartographic technician at Royal Holloway University of London, for assistance in drawing up some of the figures. We gratefully acknowledge Louis Sass and two anonymous reviewers for their helpful reviews that improved the manuscript. Open access funding enabled and organized by Projekt DEAL.

AUTHOR CONTRIBUTIONS

BD conceptualized the project with support from all co-authors. BD developed and applied the methodologies utilized, and wrote the initial draft. BD and JB mainly conducted the mapping, with assistance from CM and JC. SC, BM, MP and CM provided resources, ground-truthing and data for the project. All authors contributed to the writing and editing of the main manuscript.

DATA AVAILABILITY STATEMENT

All ESRI Shapefiles used as part of this project are available as online Supplementary Information with this article. We also provide a Supplementary A0 map showing all of the detailed mapping. All other data are included in the article. Any use of trade, firm or product names is for descriptive purposes only and does not imply endorsement by the US Government.

ORCID

Bethan Davies https://orcid.org/0000-0002-8636-1813
Tom Holt https://orcid.org/0000-0001-8361-0688
Jeremy Ely https://orcid.org/0000-0003-4007-1500

REFERENCES

Åkesson, H., Nisancioglu, K.H. & Morlighem, M. (2017) Simulating the evolution of Hardangerjøkulen ice cap in southern Norway since the mid-Holocene and its sensitivity to climate change. *The Cryosphere*, 11(1), 281–302. Available from: https://doi.org/10.5194/tc-11-281-2017

Anderson, L.S., Armstrong, W.H., Anderson, R.S. & Buri, P. (2021) Debris cover and the thinning of Kennicott Glacier, Alaska: In situ measurements, automated ice cliff delineation and distributed melt estimates. *The Cryosphere*, 15(1), 265–282. Available from: https://doi.org/10.5194/tc-15-265-2021

ASTER GDEM Validation Team, METI/ERSDAC, NASA/LPDAAC and USGS/EROS. (2009) *ASTER Global DEM Validation Summary Report*.

Azzoni, R.S., Fugazza, D., Zennaro, M., Zucali, M., D'Agata, C., Maragno, D., Cernuschi, M., Smiraglia, C. & Diolaiuti, G.A. (2017) Recent structural evolution of Forni Glacier tongue (Ortles-Cevedale Group, Central Italian Alps). *Journal of Maps*, 13(2), 870–878. Available from: https://doi.org/10.1080/17445647.2017.1394227

Barclay, D.J., Wiles, G.C. & Calkin, P.E. (2009) Holocene glacier fluctuations in Alaska. *Quaternary Science Reviews*, 28(21–22), 2034–2048. Available from: https://doi.org/10.1016/j.quascirev.2009.01.016

Barr, I.D. & Lovell, H. (2014) A review of topographic controls on moraine distribution. *Geomorphology*, 226, 44–64. Available from: https://doi.org/10.1016/j.geomorph.2014.07.030

Bendle, J.M., Thorndycraft, V.R. & Palmer, A.P. (2017) The glacial geomorphology of the Lago Buenos Aires and Lago Pueyrredón ice lobes of central Patagonia. *Journal of Maps*, 13(2), 654–673. Available from: https://doi.org/10.1080/17445647.2017.1351908

Benn, D.I. & Evans, D.J.A. (2010) *Glaciers & Glaciation*. London: Hodder Education.

Benn, D.I. & Lehmkuhl, F. (2000) Mass balance and equilibrium-line altitudes of glaciers in high-mountain environments. *Quaternary International*, 65–66, 15–29. Available from: https://doi.org/10.1016/S1040-6182(99)00034-8

Benn, D.I. & Lukas, S. (2006) Younger Dryas glacial landsystems in North West Scotland: An assessment of modern analogues and palaeoclimatic implications. *Quaternary Science Reviews*, 25(17–18), 2390–2408. Available from: https://doi.org/10.1016/j.quascirev.2006.02.015

Berthier, E., Larsen, C., Durkin, W.J., Willis, M.J. & Pritchard, M.E. (2018) Brief communication: Unabated wastage of the Juneau and Stikine icefields (southeast Alaska) in the early 21st century. *The Cryosphere*, 12(4), 1523–1530. Available from: https://doi.org/10.5194/tc-12-1523-2018

Bickerdike, H.L., Ó Cofaigh, C., Evans, D.J.A. & Stokes, C.R. (2018) Glacial landsystems, retreat dynamics and controls on Loch Lomond Stadial (Younger Dryas) glaciation in Britain. *Boreas*, 47(1), 202–224. Available from: https://doi.org/10.1111/bor.12259

Boston, C.M. & Lukas, S. (2019) Topographic controls on plateau icefield recession: Insights from the Younger Dryas Monadhliath Icefield, Scotland. *Journal of Quaternary Science*, 34(6), 433–451. Available from: https://doi.org/10.1002/jqs.3111

Boston, C.M., Lukas, S. & Carr, S.J. (2015) A Younger Dryas plateau icefield in the Monadhliath, Scotland, and implications for regional palaeoclimate. *Quaternary Science Reviews*, 108, 139–162. Available from: https://doi.org/10.1016/j.quascirev.2014.11.020

Boyce, E.S., Motyka, R.J. & Truffer, M. (2007) Flotation and retreat of a lake-calving terminus, Mendenhall Glacier, southeast Alaska, USA. *Journal of Glaciology*, 53(181), 211–224. Available from: https://doi.org/10.3189/172756507782202928

Bradwell, T., Sigurđsson, O. & Everest, J. (2013) Recent, very rapid retreat of a temperate glacier in SE Iceland. *Boreas*, 42(4), 959–973. Available from: https://doi.org/10.1111/bor.12014

Calkin, P.E. (1988) Holocene glaciation of Alaska (and adjoining Yukon Territory, Canada). *Quaternary Science Reviews*, 7(2), 159–184. Available from: https://doi.org/10.1016/0277-3791(88)90004-2

Chandler, B.M.P., Boston, C.M. & Lukas, S. (2019) A spatially-restricted Younger Dryas plateau icefield in the Gaick, Scotland: Reconstruction and palaeoclimatic implications. *Quaternary Science Reviews*, 211, 107–135. Available from: https://doi.org/10.1016/j.quascirev.2019.03.019

Chandler, B.M.P., Lovell, H., Boston, C.M., Lukas, S., Barr, I.D., Benediktsson, Í.Ö. et al. (2018) Glacial geomorphological mapping: A review of approaches and frameworks for best practice. *Earth-Science Reviews*, 185, 806–846. Available from: https://doi.org/10.1016/j.earscirev.2018.07.015

Clague, J.J., Koch, J. & Geertsema, M. (2010) Expansion of outlet glaciers of the Juneau Icefield in northwest British Columbia during the past two millennia. *The Holocene*, 20(3), 447–461. Available from: https://doi.org/10.1177/0959683609353433

Colgan, W., Rajaram, H., Abdalati, W., McCutchan, C., Mottram, R., Moussavi, M.S. et al. (2016) Glacier crevasses: Observations, models, and mass balance implications. *Reviews of Geophysics*, 54(1), 119–161. Available from: https://doi.org/10.1002/2015RG000504

Copland, L., Sharp, M.J. & Dowdeswell, J.A. (2003) The distribution and flow characteristics of surge-type glaciers in the Canadian High Arctic. *Annals of Glaciology*, 36, 73–81. Available from: https://doi.org/10.3189/172756403781816301

Cuffey, K.M. & Paterson, W.S.B. (2010) *The Physics of Glaciers*, 4th edition. New York: Academic Press.

Darvill, C.M., Stokes, C.R., Bentley, M.J., Evans, D.J.A. & Lovell, H. (2017) Dynamics of former ice lobes of the southernmost Patagonian Ice Sheet based on a glacial landsystems approach. *Journal of Quaternary Science*, 32(6), 857–876. Available from: https://doi.org/10.1002/jqs.2890

Davies, B.J., Glasser, N.F., Carrivick, J.L., Hambrey, M.J., Smellie, J.L. & Nývlt, D. (2013) Landscape evolution and ice-sheet behaviour in a semi-arid polar environment: James Ross Island, NE Antarctic Peninsula. *Geological Society of London, Special Publications*, 381(1), 353–395. Available from: https://doi.org/10.1144/SP381.1

Edwards, T.L., Nowicki, S., Marzeion, B., Hock, R., Goelzer, H., Seroussi, H. et al. (2021) Projected land ice contributions to twenty-first-century sea level rise. *Nature*, 593(7857), 74–82. Available from: https://doi.org/10.1038/s41586-021-03302-y

Evans, D.J.A. (2010) Controlled moraine development and debris transport pathways in polythermal plateau icefields: Examples from Tungnafellsjökull, Iceland. *Earth Surface Processes and Landforms*, 35(12), 1430–1444. Available from: https://doi.org/10.1002/esp.1984

Evans, D.J.A., Ewertowski, M. & Orton, C. (2016) Eiríksjökull plateau icefield landsystem, Iceland. *Journal of Maps*, 12(5), 747–756. Available from: https://doi.org/10.1080/17445647.2015.1072448

Evans, D.J.A. & Rea, B.R. (2003) Surging glacier landsystem. In: *Glacial Landsystems*. London: Taylor & Francis, pp. 259–288.

Evans, D.J.A., Rea, B.R., Hansom, J.D. & Whalley, W.B. (2002) Geomorphology and style of plateau icefield deglaciation in fjord terrains: The example of Troms-Finnmark, North Norway. *Journal of Quaternary Science*, 17(3), 221–239. Available from: https://doi.org/10.1002/jqs.675

Evans, D.J.A., Twigg, D.R. & Shand, M. (2006) Surficial geology and geomorphology of the þórisjökull plateau icefield, west-central Iceland. *Journal of Maps*, 2(1), 17–29. Available from: https://doi.org/10.4113/jom.2006.52

Furbish, D.J. & Andrews, J.T. (1984) The use of hypsometry to indicate long-term stability and response of valley glaciers to changes in mass transfer. *Journal of Glaciology*, 30(105), 199–211. Available from: https://doi.org/10.1017/S0022143000005931

Geertsema, M. & Clague, J.J. (2005) Jökulhlaups at Tulsequah Glacier, northwestern British Columbia, Canada. *The Holocene*, 15(2), 310–316. Available from: https://doi.org/10.1191/0959683605hl812rr

Glasser, N.F., Holt, T.O., Evans, Z.D., Davies, B.J., Pelto, M. & Harrison, S. (2016) Recent spatial and temporal variations in debris cover on Patagonian glaciers. *Geomorphology*, 273, 202–216. Available from: https://doi.org/10.1016/j.geomorph.2016.07.036

Glasser, N.F., Jansson, K.N., Harrison, S. & Kleman, J. (2008) The glacial geomorphology and Pleistocene history of South America between 38°S and 56°S. *Quaternary Science Reviews*, 27(3–4), 365–390. Available from: https://doi.org/10.1016/j.quascirev.2007.11.011

Glasser, N.F., Jansson, K.N., Harrison, S. & Rivera, A. (2005) Geomorphological evidence for variations of the North Patagonian Icefield during the Holocene. *Geomorphology*, 71(3–4), 263–277. Available from: https://doi.org/10.1016/j.geomorph.2005.02.003

Goodsell, B., Hambrey, M.J. & Glasser, N.F. (2002) Formation of band ogives and associated structures at Bas Glacier d'Arolla, Valais, Switzerland. *Journal of Glaciology*, 48(161), 287–300. Available from: https://doi.org/10.3189/172756502781831494

Goodsell, B., Hambrey, M.J. & Glasser, N.F. (2005) Debris transport in a temperate valley glacier: Haut Glacier d'Arolla, Valais, Switzerland. *Journal of Glaciology*, 51(172), 139–146. Available from: https://doi.org/10.3189/172756505781829647

Goodsell, B., Hambrey, M.J., Glasser, N.F., Nienow, P. & Mair, D. (2005) The structural glaciology of a temperate valley glacier: Haut Glacier d'Arolla, Valais, Switzerland. *Arctic, Antarctic and Alpine Research*, 37(2), 218–232. Available from: https://doi.org/10.1657/1523-0430(2005)037[0218:TSGOAT]2.0.CO;2

Grant, K.L., Stokes, C.R. & Evans, I.S. (2009) Identification and characteristics of surge-type glaciers on Novaya Zemlya, Russian Arctic. *Journal of Glaciology*, 55(194), 960–972. Available from: https://doi.org/10.3189/002214309790794940

Hambrey, M.J. (1977) Foliation, minor folds and strain in glacier ice. *Tectonophysics*, 39(1–3), 397–416. Available from: https://doi.org/10.1016/0040-1951(77)90106-8

Hambrey, M.J. (1994) *Glacial Environments*. London: UCL Press.

Hambrey, M.J. & Clarke, G.K.C. (2019) Structural evolution during cyclic glacier surges: 1. Structural glaciology of Trapridge Glacier, Yukon, Canada. *Journal of Geophysical Research – Earth Surface*, 124(2), 464–494. Available from: https://doi.org/10.1029/2018JF004869

Hambrey, M.J. & Lawson, W. (2000) Structural styles and deformation fields in glaciers: A review. In: Maltman, A.J., Hubbard, B. & Hambrey, M.J. (Eds.) *Deformation of Glacial Materials*. London: Geological Society of London, pp. 59–83.

Herreid, S. & Pellicciotti, F. (2020) The state of rock debris covering Earth's glaciers. *Nature Geoscience*, 13(9), 621–627. Available from: https://doi.org/10.1038/s41561-020-0615-0

Heusser, C.J. (1954) Nunatak flora of the Juneau Ice Field, Alaska. *Bulletin of the Torrey Botanical Club*, 81(3), 236–250. Available from: https://doi.org/10.2307/2481815

Heusser, C.J. & Marcus, M.G. (1964) Historical variations of Lemon Creek Glacier, Alaska, and their relationship to the climatic record. *Journal of Glaciology*, 5(37), 77–86. Available from: https://doi.org/10.1017/S0022143000028586

Heusser, C.J.B.T.-D. (2007) Chapter 2 Juneau Icefield. In: *Juneau Icefield Research Project (1949–1958)*. Amsterdam: Elsevier, pp. 15–25. https://doi.org/10.1016/S1571-0866(07)80008-X

Hock, R. & Holmgren, B. (2005) A distributed surface energy-balance model for complex topography and its application to Storglaciaren, Sweden. *Journal of Glaciology*, 51(172), 25–36. Available from: https://doi.org/10.3189/172756505781829566

Hugonnet, R., McNabb, R., Berthier, E., Menounos, B., Nuth, C., Girod, L. et al. (2021) Accelerated global glacier mass loss in the early twenty-first century. *Nature*, 592(7856), 726–731. Available from: https://doi.org/10.1038/s41586-021-03436-z

Huss, M., Hock, R., Bauder, A. & Funk, M. (2012) Conventional versus reference-surface mass balance. *Journal of Glaciology*, 58(208), 278–286. Available from: https://doi.org/10.3189/2012JoG11J216

Jacquemart, M., Loso, M., Leopold, M., Welty, E., Berthier, E., Hansen, J.S.S. et al. (2020) What drives large-scale glacier detachments? Insights from Flat Creek glacier, St. Elias Mountains, Alaska. *Geology*, 48(7), 703–707. Available from: https://doi.org/10.1130/G47211.1

Jakob, L., Gourmelen, N., Ewart, M. & Plummer, S. (2021) Spatially and temporally resolved ice loss in High Mountain Asia and the Gulf of Alaska observed by CryoSat-2 swath altimetry between 2010 and 2019. *The Cryosphere*, 15(4), 1845–1862. Available from: https://doi.org/10.5194/tc-15-1845-2021

Jennings, S.J.A. & Hambrey, M.J. (2021) Structures and deformation in glaciers and ice sheets. *Reviews of Geophysics*, 59(3), e2021RG000743. Available from: https://doi.org/10.1029/2021RG000743

Jennings, S.J.A., Hambrey, M.J. & Glasser, N.F. (2014) Ice flow-unit influence on glacier structure, debris entrainment and transport. *Earth Surface Processes and Landforms*, 39(10), 1279–1292. Available from: https://doi.org/10.1002/esp.3521

Jennings, S.J.A., Hambrey, M.J., Glasser, N.F., James, T.D. & Hubbard, B. (2016) Structural glaciology of Austre Brøggerbreen, northwest Svalbard. *Journal of Maps*, 12(5), 790–796. Available from: https://doi.org/10.1080/17445647.2015.1076744

Jiskoot, H., Curran, C.J., Tessler, D.L. & Shenton, L.R. (2009) Changes in Clemenceau Icefield and Chaba Group glaciers, Canada, related to hypsometry, tributary detachment, length–slope and area–aspect relations. *Annals of Glaciology*, 50(53), 133–143. Available from: https://doi.org/10.3189/172756410790595796

Jiskoot, H., Fox, T.A. & Van Wychen, W. (2017) Flow and structure in a dendritic glacier with bedrock steps. *Journal of Glaciology*, 63(241), 912–928. Available from: https://doi.org/10.1017/jog.2017.58

Kaufman, D.S., Young, N.E., Briner, J.P. & Manley, W.F. (2011) Alaska palaeo-glacier atlas (version 2). In: *Developments in Quaternary Sciences*. Amsterdam: Elsevier, pp. 427–445. https://doi.org/10.1016/B978-0-444-53447-7.00033-7

Kellerer-Pirklbauer, A. & Kulmer, B. (2019) The evolution of brittle and ductile structures at the surface of a partly debris-covered, rapidly thinning and slowly moving glacier in 1998–2012 (Pasterze Glacier, Austria). *Earth Surface Processes and Landforms*, 44(5), 1034–1049. Available from: https://doi.org/10.1002/esp.4552

Kienholz, C., Herreid, S., Rich, J.L., Arendt, A.A., Hock, R. & Burgess, E.W. (2015) Derivation and analysis of a complete modern-date glacier inventory for Alaska and northwest Canada. *Journal of Glaciology*, 61(227), 403–420. Available from: https://doi.org/10.3189/2015JoG14J230

Kienholz, C., Pierce, J., Hood, E., Amundson, J.M., Wolken, G.J., Jacobs, A. et al. (2020) Deglacierization of a marginal basin and implications for outburst floods, Mendenhall Glacier, Alaska. *Frontiers in Earth Science*, 8, 137. Available from: https://www.frontiersin.org/article/10.3389/feart.2020.00137

Knopf, A. (1912) The Eagle River region, southeastern Alaska. *U.S. Geological Survey Bulletin*, 502, 36–40.

Koch, J. & Clague, J.J. (2011) Extensive glaciers in northwest North America during medieval time. *Climatic Change*, 107(3–4), 593–613. Available from: https://doi.org/10.1007/s10584-010-0016-2

Kuriger, E.M., Truffer, M., Motyka, R.J. & Bucki, A.K. (2006) Episodic reactivation of large-scale push moraines in front of the advancing Taku Glacier, Alaska. *Journal of Geophysical Research – Earth Surface*, 111(F1), F01009. Available from: https://doi.org/10.1029/2005JF000385

Larsen, C.F., Motyka, R.J., Arendt, A.A., Echelmeyer, K.A. & Geissler, P.E. (2007) Glacier changes in southeast Alaska and northwest British Columbia and contribution to sea level rise. *Journal of Geophysical Research*, 112(F1), 1-11, F01007. Available from: https://doi.org/10.1029/2006jf000586

Laute, K. & Beylich, A.A. (2021) Recent glacier changes and formation of new proglacial lakes at the Jostedalsbreen Ice Cap in Southwest Norway. In: Beylich, A.A. (Ed.) *Landscapes and Landforms of Norway*. Cham: Springer International, pp. 71–95. https://doi.org/10.1007/978-3-030-52563-7_4

Lawrence, D.B. (1950) Glacier fluctuation for six centuries in southeastern Alaska and its relation to solar activity. *Geographical Review*, 40(2), 191–223. Available from: https://doi.org/10.2307/211280

Lovell, H., Fleming, E.J., Benn, D.I., Hubbard, B., Lukas, S. & Naegeli, K. (2015) Former dynamic behaviour of a cold-based valley glacier on Svalbard revealed by basal ice and structural glaciology investigations. *Journal of Glaciology*, 61(226), 309–328. Available from: https://doi.org/10.3189/2015JoG14J120

Lukas, S. (2006) Morphostratigraphic principles in glacier reconstruction – a perspective from the British Younger Dryas. *Progress in Physical Geography*, 30(6), 719–736. Available from: https://doi.org/10.1177/0309133306071955

Lüthgens, C. & Böse, M. (2012) From morphostratigraphy to geochronology – on the dating of ice marginal positions. *Quaternary Science Reviews*, 44, 26–36. Available from: https://doi.org/10.1016/j.quascirev.2010.10.009

Marcus, M.G. (1960) Periodic drainage of glacier-dammed Tulsequah Lake, British Columbia. *Geographical Review*, 50(1), 89–106. Available from: https://doi.org/10.2307/212337

Martin, J.R.V., Davies, B.J. & Thorndycraft, V.R. (2019) Glacier dynamics during a phase of Late Quaternary warming in Patagonia reconstructed from sediment–landform associations. *Geomorphology*, 337, 111–133. Available from: https://doi.org/10.1016/j.geomorph.2019.03.007

Marzeion, B., Hock, R., Anderson, B., Bliss, A., Champollion, N., Fujita, K. et al. (2020) Partitioning the uncertainty of ensemble projections of global glacier mass change. *Earth's Future*, 8(7), e2019EF001470. Available from: https://doi.org/10.1029/2019EF001470

McGrath, D., Sass, L., O'Neel, S., Arendt, A. & Kienholz, C. (2017) Hypsometric control on glacier mass balance sensitivity in Alaska and northwest Canada. *Earth's Future*, 5(3), 324–336. Available from: https://doi.org/10.1002/2016EF000479

McNeil, C., Amundson, J.M., O'Neel, S., Motyka, R.J., Sass, L., Truffer, M., Zechmann, J.M. & Campbell, S. (2021) The imminent calving retreat of Taku Glacier. *Eos, Transactions of the American Geophysical Union*, 102, Available from: https://doi.org/10.1029/2021EO154856

McNeil, C., O'Neel, S., Loso, M., Pelto, M., Sass, L., Baker, E.H. & Campbell, S. (2020) Explaining mass balance and retreat dichotomies at Taku and Lemon Creek Glaciers, Alaska. *Journal of Glaciology*, 66(258), 530–542. Available from: https://doi.org/10.1017/jog.2020.22

McNeil, C.J., Campbell, S.W., O'Neel, S. & Baker, E.H. (2019). *Glacier-Wide Mass Balance and Compiled Data Inputs: Juneau Icefield Glaciers* (vers. 2.0, January 2022). U.S. Geological Survey data release. https://doi.org/10.5066/P9YBZ36F

McNeil, C.J., Sass, L.C., Florentine, C.E., Baker, E.H., Peitzsch, E.H. & Whorton, E.N. (2016) *Glacier-Wide Mass Balance and Compiled Data Inputs: USGS Benchmark Glaciers* (vers. 6.0, January 2022). U.S. Geological Survey data release. https://doi.org/10.5066/F7HD7SRF

Millan, R., Mouginot, J., Rabatel, A. & Morlighem, M. (2022) Ice velocity and thickness of the world's glaciers. *Nature Geoscience*, 15(2), 124–129. Available from: https://doi.org/10.1038/s41561-021-00885-z

Miller, M.M. (1964) Inventory of terminal position changes in Alaskan coastal glaciers since the 1750's. *Proceedings of the American Philosophical Society*, 108, 257–273. Available from: http://www.jstor.org/stable/985682

Molnia, B.F. (2007) Late nineteenth to early twenty-first century behavior of Alaskan glaciers as indicators of changing regional climate. *Global Planetary Change*, 56(1–2), 23–56. Available from: https://doi.org/10.1016/j.gloplacha.2006.07.011

Motyka, R.J. (2003) Little Ice Age subsidence and post Little Ice Age uplift at Juneau, Alaska, inferred from dendrochronology and geomorphology. *Quaternary Research*, 59(3), 300–309. Available from: https://doi.org/10.1016/S0033-5894(03)00032-2

Motyka, R.J. & Begét, J.E. (1996) Taku Glacier, Southeast Alaska, U.S.A.: Late Holocene history of a tidewater glacier. *Arctic and Alpine Research*, 28(1), 42–51. Available from: https://doi.org/10.2307/1552084

Motyka, R.J., O'Neel, S., Connor, C.L. & Echelmeyer, K.A. (2002) Twentieth century thinning of Mendenhall Glacier, Alaska, and its relationship to climate, lake calving, and glacier run-off. *Global Planetary Change*, 35(1–2), 93–112. Available from: https://doi.org/10.1016/S0921-8181(02)00138-8

Nagorski, S.A., Kaspari, S.D., Hood, E., Fellman, J.B. & Skiles, S.M. (2019) Radiative forcing by dust and black carbon on the Juneau Icefield, Alaska. *Journal of Geophysical Research – Atmospheres*, 124(7), 3943–3959. Available from: https://doi.org/10.1029/2018JD029411

NOAA. (2021) *NOAA National Centers for Environmental Information: Climate at a Glance Series*. Available at https://www.ncdc.noaa.gov/cag/ [Accessed 17th March 2021].

Nolan, M., Motkya, R.J., Echelmeyer, K. & Trabant, D.C. (1995) Ice-thickness measurements of Taku Glacier, Alaska, USA, and their relevance to its recent behavior. *Journal of Glaciology*, 41(139), 541–553. Available from: https://doi.org/10.1017/S0022143000034870

Nye, J.F. (1952) The mechanics of glacier flow. *Journal of Glaciology*, 2(12), 82–93. Available from: https://doi.org/10.1017/S0022143000033967

Oerlemans, J. (1989) On the response of valley glaciers to climatic change. In: Oerlemans, J. (Ed.) *Glacier Fluctuations and Climatic Change*. Berlin: Springer, pp. 353–371. https://doi.org/10.1007/978-94-015-7823-3_23

O'Neel, S., McNeil, C., Sass, L.C., Florentine, C., Baker, E.H., Peitzsch, E., McGrath, D., Fountain, A.G. & Fagre, D. (2019) Reanalysis of the US Geological Survey Benchmark Glaciers: Long-term insight into climate forcing of glacier mass balance. *Journal of Glaciology*, 65(253), 850–866. Available from: https://doi.org/10.1017/jog.2019.66

Paul, F., Barrand, N.E., Baumann, S., Berthier, E., Bolch, T., Casey, K. et al. (2013) On the accuracy of glacier outlines derived from remote-sensing data. *Annals of Glaciology*, 54(63), 171–182. Available from: https://doi.org/10.3189/2013AoG63A296

Paul, F., Barry, R.G., Cogley, J.G., Frey, H., Haeberli, W., Ohmura, A. et al. (2009) Recommendations for the compilation of glacier inventory data from digital sources. *Annals of Glaciology*, 50(53), 119–126. Available from: https://doi.org/10.3189/172756410790595778

Paul, F., Bolch, T., Briggs, K., Kääb, A., McMillan, M., McNabb, R. et al. (2017) Error sources and guidelines for quality assessment of glacier area, elevation change, and velocity products derived from satellite data in the Glaciers_cci project. *Remote Sensing of Environment*, 203, 256–275. Available from: https://doi.org/10.1016/j.rse.2017.08.038

Pelto, M. (2019) Exceptionally high 2018 equilibrium line altitude on Taku Glacier, Alaska. *Remote Sensing*, 11(20), 2378. Available from: https://doi.org/10.3390/rs11202378

Pelto, M., Kavanaugh, J. & McNeil, C. (2013) Juneau Icefield mass balance program 1946–2011. *Earth System Science Data*, 5(2), 319–330. Available from: https://doi.org/10.5194/essd-5-319-2013

Pfeffer, W.T., Arendt, A.A., Bliss, A., Bolch, T., Cogley, J.G., Gardner, A.S. et al. (2014) The Randolph Glacier Inventory: A globally complete inventory of glaciers. *Journal of Glaciology*, 60(221), 537–552. Available from: https://doi.org/10.3189/2014JoG13J176

Porter, C., Morin, P., Howat, I., Noh, M.-J., Bates, B., Peterman, K. et al. (2018) ArcticDEM. *Harvard Dataverse* 1.

Porter, S.C. (2013) GLACIATIONS|Neoglaciation in the American Cordilleras. In: Elias, S.A. (Ed.) *Encyclopedia of Quaternary Science*, 2nd edition. Amsterdam: Elsevier, pp. 269–276. https://doi.org/10.1016/B978-0-444-53643-3.00127-8

Randolph Glacier Inventory Consortium, Arendt, A., Bliss, A., Bolch, T., Cogley, J.G., Gardner, A. et al. (2017) *Randolph Glacier Inventory – a dataset of global glacier outlines: Version 6.0. Technical report, global land ice measurements from space, Colorado, USA*. Digital media.

Rau, F., Mauz, F., Vogt, S., Khalsa, S.J.S. & Raup, B. (2005) *Illustrated GLIMS Glacier Classification Manual, Version 1.0*. GLIMS Regional Centre, "Antarctic Peninsula": GLIMS (Global Land Ice Measurement from Space), NSIDC.

Rippin, D.M., Sharp, M., Van Wychen, W. & Zubot, D. (2020) 'Detachment' of icefield outlet glaciers: Catastrophic thinning and retreat of the Columbia Glacier (Canada). *Earth Surface Processes and Landforms*, 45(2), 459–472. Available from: https://doi.org/10.1002/esp.4746

Rootes, C.M. & Clark, C.D. (2020) Glacial trimlines to identify former ice margins and subglacial thermal boundaries: A review and classification scheme for trimline expression. *Earth-Science Review*, 210, 103355. Available from: https://doi.org/10.1016/j.earscirev.2020.103355

Roth, A., Hock, R., Schuler, T.V., Bieniek, P.A., Pelto, M. & Aschwanden, A. (2018) Modeling winter precipitation over the Juneau Icefield, Alaska, using a linear model of orographic precipitation. *Frontiers in Earth Science*, 6, Available from: https://doi.org/10.3389/feart.2018.00020

Röthlisberger, F. (1986) *10,000 Jahre Gletschergeschichte der Erde*. Aarau: Sauerlander.

Sass, L.C., Loso, M.G., Geck, J., Thoms, E.E. & McGrath, D. (2017) Geometry, mass balance and thinning at Eklutna Glacier, Alaska: An altitude-mass-balance feedback with implications for water resources. *Journal of Glaciology*, 63(238), 343–354. Available from: https://doi.org/10.1017/jog.2016.146

Seguinot, J., Rogozhina, I., Stroeven, A.P., Margold, M. & Kleman, J. (2016) Numerical simulations of the Cordilleran Ice Sheet through the last glacial cycle. *The Cryosphere*, 10(2), 639–664. Available from: https://doi.org/10.5194/tc-10-639-2016

Shannon, S., Smith, R., Wiltshire, A., Payne, T., Huss, M., Betts, R. et al. (2019) Global glacier volume projections under high-end climate change scenarios. *The Cryosphere*, 13(1), 325–350. Available from: https://doi.org/10.5194/tc-13-325-2019

Slater, T., Lawrence, I.R., Otosaka, I.N., Shepherd, A., Gourmelen, N., Jakob, L. et al. (2021) Review article: Earth's ice imbalance. *The Cryosphere*, 15, 233–246. Available from: https://doi.org/10.5194/tc-15-233-2021

Sprenke, K.F., Miller, M.M., McGee, S.R., Adema, G.W. & Lang, M. (1999a) CANADIAN LANDFORM EXAMPLES - 36: THE HIGH ICE PLATEAU OF THE JUNEAU ICEFIELD, BRITISH COLUMBIA: FORM AND DYNAMICS. *The Canadian Geographer/Le Géographe canadien*, 43(1), 99–104. Available from: https://doi.org/10.1111/j.1541-0064.1999.tb01363.x

Sprenke, K.F., Miller, M.M., McGee, S.R., Adema, G.W. & Lang, M. (1999b) The high ice plateau of the Juneau Icefield, British Columbia: Form and dynamics. *Canadian Geographic*, 43(1), 99–104. Available from: https://doi.org/10.1111/j.1541-0064.1999.tb01363.x

Stone, K.H. (1963) Alaskan ice-dammed lakes. *Annals of the Association of American Geographers*, 53(3), 332–349. Available from: https://doi.org/10.1111/j.1467-8306.1963.tb00453.x

Thoman, R. & Walsh, J.E. (2019) *Alaska's Changing Environment: Documenting Alaska's Physical and Biological Changes Through Observations*. International Arctic Research Center, University of Alaska Fairbanks: Fairbanks, AL.

Veitch, S.A., Karplus, M., Kaip, G., Gonzalez, L.F., Amundson, J.M. & Bartholomaus, T.C. (2021) Ice thickness estimates of Lemon Creek Glacier, Alaska, from active-source seismic imaging. *Journal of Glaciology*, 67(265), 824–832. Available from: https://doi.org/10.1017/jog.2021.32

Weber, P., Boston, C.M., Lovell, H. & Andreassen, L.M. (2019) Evolution of the Norwegian plateau icefield Hardangerjøkulen since the 'Little Ice Age'. *The Holocene*, 29, 1885–1905. Available from: https://doi.org/10.1177/0959683619865601

Wentworth, C.K. & Ray, L.L. (1936) Studies of certain Alaskan glaciers in 1931. *Geological Society of America Bulletin*, 47(6), 879–934. Available from: https://doi.org/10.1130/GSAB-47-879

Wiles, G.C., Barclay, D.J. & Calkin, P.E. (1999) Tree-ring-dated 'Little Ice Age' histories of maritime glaciers from western Prince William Sound, Alaska. *The Holocene*, 9(2), 163–173. Available from: https://doi.org/10.1191/095968399671927145

Zekollari, H., Huybrechts, P., Noël, B., van de Berg, W.J. & van den Broeke, M.R. (2017) Sensitivity, stability and future evolution of the world's northernmost ice cap, Hans Tausen Iskappe (Greenland). *The Cryosphere*, 11(2), 805–825. Available from: https://doi.org/10.5194/tc-11-805-2017

Zemp, M., Huss, M., Thibert, E., Eckert, N., McNabb, R., Huber, J. et al. (2019) Global glacier mass changes and their contributions to sea-level rise from 1961 to 2016. *Nature*, 568(7752), 382–386. Available from: https://doi.org/10.1038/s41586-019-1071-0

Ziemen, F.A., Hock, R., Aschwanden, A., Khroulev, C., Kienholz, C., Melkonian, A. et al. (2016) Modeling the evolution of the Juneau Icefield between 1971 and 2100 using the Parallel Ice Sheet Model (PISM). *Journal of Glaciology*, 62(231), 199–214. Available from: https://doi.org/10.1017/jog.2016.13

SUPPORTING INFORMATION

Additional supporting information may be found in the online version of the article at the publisher's website.

How to cite this article: Davies, B., Bendle, J., Carrivick, J., McNabb, R., McNeil, C., Pelto, M. et al. (2022) Topographic controls on ice flow and recession for Juneau Icefield (Alaska/British Columbia). *Earth Surface Processes and Landforms*, 47(9), 2357–2390. Available from: https://doi.org/10.1002/esp.5383